

1 Structure and deformation of the Kermadec forearc in response to subduction of  
2 the Pacific oceanic plate

3  
4 Funnell<sup>1</sup>, M.J., Peirce<sup>1</sup>, C., Stratford<sup>1</sup>, W.R., Paulatto<sup>2,4</sup>, M., Watts<sup>2</sup>, A.B. and Grevemeyer<sup>3</sup>, I.

5  
6 <sup>1</sup> Department of Earth Sciences, Durham University, South Road, Durham, DH1 3LE, UK.

7 Email: matthew.funnell2@durham.ac.uk

8 <sup>2</sup> Department of Earth Sciences, University of Oxford, Oxford, OX1 3PR, UK.

9 <sup>3</sup> GEOMAR, Helmholtz Centre of Ocean Research, 24148 Kiel, Germany.

10 <sup>4</sup> Géoazur, Bât 4, 250 Rue Albert Einstein, Les Lucioles 1, Sophia-Antipolis, 06560 Valbonne, France.

11  
12  
13 Accepted

Received

in original form

14  
15 **SUMMARY**

16 The Tonga-Kermadec forearc is deforming in response to on-going subduction of the Pacific plate  
17 beneath the Indo-Australian plate. Previous research has focussed on the structural development of the  
18 forearc where large bathymetric features such as the Hikurangi Plateau and Louisville Ridge seamount  
19 chain are being subducted. Consequently, knowledge of the “background” forearc in regions of normal  
20 plate convergence is limited. We report on an ~250 km-long multichannel seismic reflection profile  
21 that was shot perpendicular to the Tonga-Kermadec trench at ~28°S to determine the lateral and  
22 temporal variations in the structure, stratigraphy and deformation of the Kermadec forearc resulting  
23 solely from Pacific plate subduction.

24 Interpretation of the seismic profile, in conjunction with regional swath bathymetry data,  
25 shows that the Pacific plate exhibits horst and graben structures that accommodate bending-induced  
26 extensional stresses, generated as the trenchward dip of the crust increases. Trench infill is also much  
27 thicker than expected at 1 km which, we propose, results from increased sediment flux into and along  
28 the trench. Pervasive normal faulting of the mid-trench slope most likely accommodates the majority  
29 of the observed forearc extension in response to basal subduction erosion, and a structural high is  
30 located between the mid- and upper-trench slopes. We interpret this high as representing a dense and  
31 most likely structurally robust region of crust lying beneath this region.

32 Sediment of the upper-trench slope documents depositional hiatuses and on-going uplift of the  
33 arc. Strong along-arc currents appear to erode the Kermadec volcanic arc and distribute this sediment  
34 to the surrounding basins, while currents over the forearc redistribute deposits as sediment waves.  
35 Minor uplift of the transitional Kermadec forearc, observed just to the north of the profile, appears to  
36 relate to an underlying structural trend as well as subduction of the Louisville Ridge seamount chain  
37 250 km to the north. Relative uplift of the Kermadec arc is observed from changes in the tilt of upper-  
38 trench slope deposits and extensional faulting of the basement immediately surrounding the Louisville  
39 Ridge.

40  
41 **Key words:** Subduction zone processes, controlled-source seismology, dynamics and mechanics of  
42 faulting, fractures and faults.

## 43 **1 INTRODUCTION**

44 Subduction of the Pacific plate occurs along 2,700 km of the Tonga-Kermadec trench (Fig. 1). This  
45 classic example of an intra-oceanic, non-accretionary and erosional convergent plate margin exhibits  
46 the fastest rates of convergence and the most linear trench-forearc complex of the global subduction  
47 system (Brodie & Hatherton, 1958; Dickinson & Seely, 1979; Bevis *et al.*, 1995). Since the Pacific  
48 plate began to subduct beneath the Indo-Australian plate in the Mid-Eocene, the Tonga-Kermadec  
49 forearc and arc have developed into the multi-component system seen today (Hawkins *et al.*, 1984;  
50 Clift *et al.*, 1998). The Kermadec trench and forearc, which comprise the southern section of this  
51 subduction system, are separated from the Tonga trench to the north, and the Hikurangi trench to the  
52 south, by subduction of the Louisville Ridge seamount chain (LRSC) and Hikurangi Plateau  
53 respectively (Ballance *et al.*, 1989; Davy, 1992).

54 Forearcs evolve in response to changes in the rate, angle and obliquity of subduction as well  
55 as the strength and roughness of the subducting plate (Dickinson & Seely, 1979; von Huene & Scholl,  
56 1991). Variations in these characteristics often manifest themselves as changes in the dominant stress  
57 regime (Bonnardot *et al.*, 2007), and the rate of frontal and basal subduction erosion of the overriding  
58 plate (Clift & Vannucchi, 2004; von Huene *et al.*, 2004). The LRSC and Hikurangi Plateau are  
59 thickened and buoyant regions of oceanic lithosphere, whose subduction is observed to have had a  
60 significant effect on the structural development of the forearc of the overriding plate (Collot & Davy,  
61 1998; Davy & Collot, 2000; Contreras-Reyes *et al.*, 2011; Stratford *et al.*, 2014). Despite numerous  
62 investigations of the subduction and forearc deformation processes to the north and south, the structure  
63 of the Kermadec trench and forearc are constrained only by spatially restricted swath bathymetry and  
64 low resolution, single channel seismic reflection data (Karig, 1970; Dickinson & Seely, 1979; Katz,  
65 1981; Herzer *et al.*, 1984). As a result, the subsurface structure of the Kermadec trench and forearc  
66 remains poorly understood, and little is known of the sedimentation and deformation processes that  
67 have influenced forearc development since subduction initiation.

68 In 2011, wide-angle seismic refraction and multichannel seismic (MCS) reflection data were  
69 acquired, together with Parasound, gravity, magnetic, swath bathymetry and backscatter data, along  
70 profiles crossing the Tonga-Kermadec trench-arc system (Peirce & Watts, 2011). This study uses data  
71 acquired along Profile D, which crosses the trench at  $\sim 28^{\circ}\text{S}$ , to better understand Kermadec forearc  
72 structure, principal deformation styles and their lateral variations between  $26.5^{\circ}\text{S}$  and  $30^{\circ}\text{S}$  by: (i)  
73 imaging the stratigraphy and structures of the subducting and overriding plates; (ii) determining how  
74 sediments are transported and deposited across the different regions of the trench-forearc system, and  
75 how this has changed over time; (iii) resolving structural features in the MCS, Parasound and swath  
76 bathymetry data to understand along-profile forearc deformation; and (iv) relating these sedimentary  
77 and deformation processes to trends and variations in the bathymetric characteristics of the outer- and  
78 inner-trench slopes of the Tonga-Kermadec subduction system. A discussion of the changes in forearc  
79 deformation and structures caused by seamount subduction at the Tonga-Kermadec subduction system  
80 can be found in Stratford *et al.* (2014).

## 81 2 GEOLOGICAL SETTING

82 The tectonic history of the Tonga-Kermadec subduction system is both multi-stage and complex  
83 (Parson *et al.*, 1992). Although the present-day volcanic arcs originated closer to their respective  
84 trenches (Clift & MacLeod, 1999), they have supplied volcanoclastic material to the surrounding  
85 basins since the Eocene (Sutherland, 1995). Subduction of the Pacific plate initiated in the middle  
86 Eocene (~44 Ma – McDougall, 1994; Bloomer *et al.*, 1995), causing the inner forearc slope to rise ~1  
87 km, and the trench to depress to its current depth (Ballance *et al.*, 1989; Parson *et al.*, 1992). The  
88 abundance of volcanoclastic material, dated as late Miocene in age, implies the presence of a single  
89 volcanic chain before this time (Ballance *et al.*, 1989). This single-arc system remained stable until  
90 rifting of the Lau Basin began at ~7.8 Ma (Clift, 1994; Ballance *et al.*, 1999), and the Havre Trough  
91 opened ~5 Ma (Malahoff *et al.*, 1982, Clift *et al.*, 1994). Initiation of rifting in these backarc basins  
92 coincides with a peak in the generation of volcanoclastic material. An ~2 Myr regional hiatus in  
93 sedimentation followed this increased volcanic output (Clift, 1994; Ballance *et al.*, 1999). Tectonic  
94 erosion of the overriding plate has progressively extended and depressed the Tonga forearc by ~280%  
95 and ~6 km respectively since the Miocene (MacLeod, 1994; Clift *et al.*, 1994). These changes, relative  
96 to the effectively static depth of the volcanic arc with time, cause the forearc to rotate towards the  
97 trench (Clift & MacLeod, 1999).

98 The Pacific and Indo-Australian plates converge at rates of up to 164–249 mm yr<sup>-1</sup> along the  
99 Tonga-Kermadec subduction system (Bevis *et al.*, 1995). An 020° trending trench axis, with a mean  
100 depth of ~8 km (Ballance *et al.*, 1989), delimits the zone where old (~80 Ma) and dense Pacific plate  
101 is thrust beneath the Indo-Australian plate (Lonsdale, 1988) (Fig. 1). Along this subduction zone the  
102 crust and mantle of the Pacific oceanic lithosphere is most likely hydrated through new bend-related  
103 faults that are generated across the outer rise (Ranero *et al.*, 2003). Fast rates of convergence and the  
104 hydration of this cold and brittle oceanic lithosphere cause the Tonga-Kermadec subduction system to  
105 be one of the most seismically and volcanically active in the global subduction system (Bevis *et al.*,  
106 1995; Grevemeyer *et al.*, 2005).

107 Trench-parallel normal faults form in the poorly sedimented underthrusting (down-going)  
108 plate as it passes over the outer rise and bends towards the trench (Lonsdale, 1986; MacLeod, 1994).  
109 Ballance *et al.* (1989) and MacLeod (1994) proposed that arc-derived volcanoclastic sediments,  
110 transported via submarine canyons, dominate the fill of the graben structures as they subduct. This  
111 process is observed along the sediment-starved convergent margin off northern Chile, and is  
112 supplemented by the addition of crustal material disaggregated from the forearc basement (von Huene  
113 & Ranero, 2003, Ranero *et al.*, 2006, Maksymowicz *et al.*, 2012). Although the lack of sediments on  
114 the subducting plate prevents the formation of an accretionary wedge along the northern Chile and  
115 Tonga-Kermadec subduction zones, the abundance of forearc-derived material along the northern  
116 Chile margin generates a frontal prism under a compressive regime (Shreve & Cloos, 1986; von  
117 Huene & Ranero, 2003).

118           Currently, the structure and morphology of the Tonga-Kermadec trench-forearc system varies  
119 significantly along its length (Fig. 1). A steeply dipping (10–24°) and highly irregular basement with  
120 little sediment cover characterises the inner-trench slope (Karig, 1970; Ballance *et al.*, 1999). Poor  
121 sedimentation of the trench and inner slope is a consequence of reduced sediment transport, which  
122 results from sediment ponding in basins located higher up on the forearc (Dickinson & Seely, 1979).  
123 Mid-slope terraces, for example, act as effective sediment traps and are located along the length of the  
124 Tonga-Kermadec forearc at ~5-6 km water depth (e.g. Brodie & Hatherton, 1958; Karig, 1970;  
125 Ballance *et al.*, 1999). Extension in the lower- and middle-trench slopes has been inferred from the  
126 presence of normal faults observed in cores at ODP Site 841 (Fig. 1 – MacLeod, 1994) and low  
127 seismic velocity regions modelled from wide-angle seismic refraction data (Contreras-Reyes *et al.*,  
128 2011; Stratford *et al.*, 2014). This extensional zone is associated with the presence of an ~2,000 km-  
129 long scarp, more prominent in the Tonga forearc than the Kermadec forearc, located ~60 km behind  
130 the trench (Contreras-Reyes *et al.*, 2011). von Huene *et al.* (2004) hypothesise that such extension, and  
131 thus subsidence, of the lower- and mid-trench slopes results from the hydrofracturing and subsequent  
132 removal of basal material from the overthrusting plate.

133           Single channel seismic reflection data from Karig (1970) indicate that the Kermadec forearc is  
134 dominated by a thick sedimentary succession, which is divided into two clear units by a bright  
135 reflection event. The Karig (1970) data failed to image the internal structure of the deposits of the  
136 upper forearc, and so they were described as acoustically transparent. Clift *et al.* (1994) recognised full  
137 Bouma sequences (Bouma, 1962) in cores at ODP site 840, located on the Tonga Platform (Fig. 1),  
138 and speculated that turbidite flows dominate sedimentation on the upper-trench slopes.

139           Formed by volcanism related to the subduction of thinly sedimented crust (Ballance *et al.*,  
140 1989; Castillo *et al.*, 2009), the Tonga and Kermadec arcs lie ~200 km west of their respective  
141 trenches. These volcanic chains are elevated significantly above the surrounding forearc and backarc,  
142 allowing distribution of volcanoclastic material to the adjacent basins (Brodie & Hatherton, 1958;  
143 Karig, 1970). These volcanic arcs are continually being uplifted (Ballance *et al.*, 1989). Strike-slip and  
144 normal fault systems found on the western slope of the Tonga and Kermadec arcs reflect their oblique  
145 angle of subduction (Bonnardot *et al.*, 2007), while on-going extension in the Lau Basin and Havre  
146 Trough causes increasing separation of the arcs from their respective backarcs (Delteil *et al.*, 2002).

147           There are two major changes in tectonic regime along the length of the subduction system. At  
148 ~26°S, an observed reduction in shallow seismicity coincides with the collision of the LRSC and the  
149 Tonga-Kermadec trench (Haberman *et al.*, 1986). Geochemical anomaly data obtained from lavas  
150 located at ~22°S on the Tonga Arc, north of the present-day LRSC collision zone, indicate that  
151 subduction of the LRSC initiated at least 7 Ma (Timm *et al.*, 2013). The most northwesterly and  
152 currently subducting seamount of the volcanic chain (which are commonly ~2 km high and 10-40 km  
153 in diameter) causes a bathymetric discontinuity in the trench and at the lower-trench slope (Lonsdale,  
154 1988). This discontinuity divides the Tonga trench-forearc system to the north from the Kermadec  
155 trench-forearc system in the south (Karig, 1970; Pelletier & Dupont, 1990), and causes segmentation

156 into the different tectonic regimes (Bonnardot *et al.*, 2007). The oblique strike (335°) of the 4,300 km-  
157 long seamount chain and the oblique plate convergence, cause the point of collision to migrate  
158 southward at ~180 mm yr<sup>-1</sup> (Ballance *et al.*, 1989). Thus, the Tonga forearc has experienced the effects  
159 of LRSC subduction, whereas the Kermadec forearc has not.

160 Subduction of the LRSC elevates and then lowers the overriding forearc, causing it to be  
161 faulted and thus weakened (Clift & MacLeod, 1999). This process is thought to constitute the majority  
162 of subduction erosion that is observed at this boundary, surpassing that which normally occurs at the  
163 front and base of the overriding plate as Pacific oceanic crust is subducted (von Huene & Scholl, 1991;  
164 Clift & Vannucchi, 2004). The effect of this increased and accelerated tectonic erosion is manifest in  
165 the significant loss of forearc material over a short period of time (estimated to be ~80 km<sup>3</sup> – Clift &  
166 MacLeod, 1999), and observed as a substantial thinning and shortening of the forearc, which results in  
167 an increase in slope gradient (Ballance *et al.*, 1989).

168 The second major tectonic boundary occurs at 32°S along the Kermadec trench, where Karig  
169 (1970) first noted an anomalous increase in trench depth to the south. There is a coincident 10 km  
170 westward step in the forearc (Pelletier & Dupont, 1990), together with significant increases in the  
171 depth and narrowing of the mid-slope terrace (Ballance *et al.*, 1999). An increase in the dip angle of  
172 the subducting plate is thought to cause these variations that, in turn, progressively rotate the forearc  
173 trenchward (Ballance *et al.*, 1999). This 32°S boundary is also associated with the partitioning on the  
174 western slope of the Kermadec forearc of strike-slip and normal faulting, to the north and south  
175 respectively (Bonnardot *et al.*, 2007).

176

### 177 **3 DATA ACQUISITION AND PROCESSING**

178 The ~250 km-long MCS profile traversing the Kermadec subduction system south of the LRSC  
179 collision zone was acquired from the 29<sup>th</sup> April to 1<sup>st</sup> May 2011 as part of *R/V Sonne* cruise SO215  
180 (Peirce & Watts, 2011), which followed on from the *Tonga Thrust* earthquake *Asperity* at Louisville  
181 Ridge (TOTAL) project (Grevemeyer & Flüh, 2008). This MCS line, Profile D in Peirce & Watts  
182 (2011), was located to study “background” processes and structures associated with the subduction of  
183 Pacific oceanic lithosphere uninfluenced by LRSC subduction. The profile runs perpendicular to the  
184 trench-arc system, from ~50 km to the east of the trench to 35 km west of the present-day Kermadec  
185 arc (Fig. 2). Gravity, magnetic, Parasound and multibeam bathymetry data were acquired  
186 contemporaneously.

187 The seismic source consisted of a 10 G-gun array, with a combined volume of 4400 in<sup>3</sup> (68 l),  
188 which was towed at a depth of 7.5 m and fired at a pressure of 2400 psi (170 bar). Shots were fired  
189 every 30 s which, at the ship speed of ~4.5 kn, resulted in an ~70 m interval between shots. The  
190 acquisition system also included a 3 km multichannel streamer, comprising 240 channels at 12.5 m  
191 group interval, towed at 10 m depth. The dataset collected consists of 29 s long traces, recorded at a  
192 sampling rate of 1 ms. Each common midpoint (CMP), separated by 6.25 m, has a maximum  
193 theoretical fold of ~20.

194 Initial analysis of the MCS data indicated a low signal-to-noise ratio, as might be expected of  
195 a subduction zone where the seabed is rough and scattering, and the sub-surface geology is complex.  
196 By grouping the CMPs into 25 m bins, the fold was increased from ~20 to ~80 and significantly  
197 improved the signal-to-noise ratio, whilst also reducing variations in CMP spacing caused by shooting  
198 the profile at specific shot times rather than on intra-shot distance. Increased CMP bin sizes also  
199 improve the resolution of the MCS data at depth. Although increasing the bin size is undertaken at the  
200 expense of optimum horizontal resolution, interpretation of the final stacked section is not affected  
201 because the seafloor and subsurface structures are still significantly larger than the increased CMP  
202 spacing.

203 A simple processing scheme was applied comprising velocity analysis, stacking, post-stack  
204 deconvolution, bandpass filtering and migration. Detailed velocity analysis, required to ensure that  
205 lateral changes in seafloor relief and sub-seabed velocity variations are correctly represented in the  
206 velocity model, was conducted using a combination of semblance, constant velocity stacks and gathers,  
207 and undertaken at intervals of 25 CMPs (fewer in more structurally complex regions). Well-  
208 constrained velocity picks were possible throughout the sedimentary units. However, the lack of sub-  
209 basement (crustal) reflections resulted in a simple velocity gradient being applied below the basement.  
210 The assumption of a velocity gradient from the top of the basement to the bottom of the seismic  
211 section is inconsequential to later interpretation given the absence of observable sub-basement primary  
212 reflections. Post-stack deconvolution sharpened the wavelet, and effectively removed a short-path  
213 multiple delayed ~220 ms behind the primary reflection. The deconvolution operator was designed  
214 using the primary reflection generated by a horizontal and planar region of seabed overlying a unit of  
215 flat-lying sediments. A Butterworth filter (bandpass range: 3-10-100-120 Hz) reduced noise outside of  
216 the useful data bandwidth; in particular the low frequency, high amplitude wave noise recorded during  
217 rougher sea states. The application of a post-stack, constant velocity ( $1500 \text{ m s}^{-1}$ ) Kirchhoff migration  
218 reduced the appearance of high amplitude diffraction tails generated by the rough seabed. For display  
219 purposes, a mute was applied before the primary seabed reflection, and a long time-gate (2000 ms)  
220 automatic gain control (AGC) equalised reflection amplitudes along each trace. The MCS data were  
221 not time-to-depth converted due to a lack of actual velocity control other than stacking velocities  
222 derived from velocity analysis.

223 High-resolution, shallow sub-seabed imaging data, collected by the shipboard Atlas Parasound  
224 P70, were recorded in ~800 ms windows around the seabed. The recording delay was determined by  
225 the swath-derived seabed depth, and stored in the SEG-Y headers. Application of a bandpass filter  
226 (2.0-2.5-5.5-6.0 kHz) around the dominant signal frequency of 4 kHz reduced noise, and an AGC of  
227 200 ms improved the appearance for display.

228 A shipboard SIMRAD EM120 multibeam echo sounding system acquired swath bathymetry  
229 data throughout the cruise. Processing of the raw data in MB-System included the flagging of data that  
230 had deviated from the local median depth by more than 100 m between beams to enable the removal  
231 of bathymetric artefacts introduced during acquisition (Caress & Chayes, 1999). The cleaned swath

232 bathymetry and backscatter amplitude data were gridded at 50 m intervals before being merged with  
233 existing ship-track data to produce an updated, but still sparse, high-resolution map of the seafloor  
234 (Fig. 2). These data were then combined with the General Bathymetric Chart of the Oceans (GEBCO -  
235 IOC *et al.*, 2003) 30 arc-second grid to provide a more complete regional bathymetric map (Fig. 1).

236

#### 237 **4 INTERPRETATIVE DISCUSSION**

238 Profile D crosses the Kermadec trench at  $\sim 28^{\circ}\text{S}$  (Fig. 1). At this location, processes associated with  
239 the subduction of background Pacific oceanic lithosphere should cause the majority of deformation to  
240 the Kermadec forearc. In this section, a detailed interpretation of Profile D (Fig. 2) focuses on the  
241 structure and stratigraphy of the major units that comprise the Kermadec trench-arc system. This  
242 interpretation is then related to Parasound sub-seabed images and bathymetry maps to draw  
243 conclusions about the on-going deformation throughout the background Kermadec trench region. Fig.  
244 2 shows where each of the following figures, which display specific structural regions and features in  
245 detail, are located along Profile D. For ease of correlation, all “depth” and “thickness” estimates are  
246 reported in two-way traveltime (TWTT). Comparisons of these data with Profile A (Peirce & Watts,  
247 2011), which images structures and deformation of the Tonga forearc associated with LRSC  
248 subduction, are made in Stratford *et al.* (2014).

249

##### 250 *4.1 General overview of Profile D*

251 The subducting Pacific oceanic plate is characterised by a thin cover of sediment ( $<0.2$  s TWTT thick)  
252 and extensive normal faulting. This old oceanic plate, imaged along the easternmost 50 km of Profile  
253 D, enters the trench at a water depth of 12.4 s TWTT ( $\sim 9300$  m). Despite being clearly imaged across  
254 the  $\sim 5$  km wide and sediment-filled (up to 1 s TWTT) trench, the seismic reflection response of the  
255 down-going plate reduces significantly as it begins to underthrust beneath the overthrusting Indo-  
256 Australian plate.

257 The overthrusting Indo-Australian plate can be subdivided into five major structural units: the  
258 lower-trench slope; mid-trench slope; upper-trench slope with associated forearc basin; the Kermadec  
259 arc; and the Lau-Havre backarc basin (Fig. 2). For 20 km west of the trench, the irregular morphology  
260 of the lower-trench slope shallows steeply ( $\sim 10^{\circ}$ ) to 6.7 s TWTT ( $\sim 5000$  m) water depth. A decrease  
261 in bathymetric gradient and thickening of the sedimentary sequence characterises the transition from  
262 the lower- to mid-trench slope at  $\sim 6$  s TWTT. Further west, the mid-trench slope consists of a 25 km-  
263 wide plateau and adjacent slope. The structure of the basement of the mid-trench slope is not  
264 concordant with seabed features, implying a complex structural history. The slope to the west of the  
265 plateau shallows by 2.1 s TWTT to form a forearc structural high. From here the upper-trench slope  
266 rises for  $\sim 70$  km into the arc. The forearc basin, situated on the upper-trench slope, is characterised by  
267 sediments that reach their thickest ( $\sim 2$  s TWTT) towards the centre of the slope region (175-185 km  
268 offset). At the western limit of the upper-trench slope ( $\sim 210$  km offset), the forearc shallows to a water  
269 depth of 1.45 s TWTT ( $\sim 1100$  m). Although no active volcano is present at the latitude of Profile D,

270 this section of the Kermadec Ridge is coincident with an active volcanic arc (Karig, 1970). Profile D  
271 images ~30 km of the backarc slope, which displays sediment cover averaging 1 s TWTT thick.

272

#### 273 *4.2 Pacific oceanic plate*

274 Fig. 3 displays the extent of the Pacific plate imaged along Profile D (~50 km). The down-going  
275 oceanic lithosphere exhibits uniform but thin sediment cover (~0.2 s TWTT – see Fig. 3a inset).  
276 Seabed and intra-sediment reflections, concordant with those of the top of the crust, indicate steady  
277 and laterally consistent deposition. These deposits are likely to be dominated by pelagic sediments that  
278 have accumulated since the crust formed ~80 Ma; however, they may also include thin successions of  
279 volcanoclastic sediments introduced by the LRSC and Kermadec arc volcanic centres, such as those  
280 observed at ODP site 204 (Burns *et al.*, 1973).

281 On Profile D, the lateral continuity of the reflections that characterise the Pacific plate is  
282 limited by normal faults of a range of scales (from <0.05 to 0.8 s TWTT offset – Fig. 3b). Lonsdale  
283 (1986) and Aubouin (1989) note that these extensional structures form when oceanic crust passes over  
284 the flexural bulge of the subducting plate, giving rise to an ~80 km wide fault zone. Fault offsets and  
285 the dip angle of the plate increase to ~2 km and ~5° respectively with proximity to the trench (Figs 3b  
286 & e). These faults form in response to the dominant formation stress, which is a bend-induced tension  
287 (Caldwell *et al.* 1976), and grow as the tension intensifies (to several kilobars) effectively relaxing the  
288 stresses applied to the crust and uppermost mantle of the subducting oceanic plate in regions of high  
289 curvature (Watts *et al.*, 1980).

290 Swath bathymetry data from the region indicate that the horst and graben structures on the  
291 down-going plate trend between 010-030° (Fig. 3e). This roughly trench-parallel fabric extends along  
292 the length of the Tonga-Kermadec subduction system, and is broken into 50-200 km-long segments,  
293 approximately 5-15 km in width. These horst and graben characteristics are similar to those observed  
294 at other examples of bend-related faulting from around the Pacific, such as offshore Nicaragua  
295 (Ranero *et al.*, 2003; Grevemeyer *et al.*, 2005). The trench-parallel trend of these bend faults is  
296 perpendicular to the fabric of formation for Pacific oceanic lithosphere at this latitude (Billen & Stock,  
297 2000), supporting the hypothesis that new faults will form parallel to the trench in oceanic lithosphere  
298 if the fabric of formation is >25° from the trend of the trench (Billen *et al.*, 2007). Approximately 150  
299 km south of the LRSC collision zone, deformation of the subducting plate appears to partition. South  
300 of this point, minor variations in the fault trend and structure show no coherency. However, to the  
301 north, the vertical offset of these faulting structures reduces considerably, causing the trench axis to  
302 shallow by ~4.5 km towards the current point of collision with the LRSC (Pontoise *et al.*, 1986). For  
303 example, compare seabed depths at <75 and >225 km offset perpendicular to Profile D in Fig. 3e.  
304 Thus, we define the subduction of purely background Pacific oceanic plate as that which occurs  
305 further than 150 km south of the present-day LRSC-trench collision point, and note that north of this  
306 boundary, the bathymetry of the trench axis gradually shallows until the LRSC is reached.

307

### 308 4.3 Trench fill

309 Along Profile D, the sediment fill of the 5 km-wide trench exhibits reflection characteristics that vary  
310 significantly over the lateral extent of the trench (shown in detail in Fig. 3c). Towards the east,  
311 reflections are relatively horizontal and planar, displaying slight onlap onto the subducting crust.  
312 However, further west these same reflections adopt vertically stacked concave-up structures (~2 km  
313 wide), and are covered by a wedge of sediment that thickens with proximity to the overriding plate.  
314 This high-angle wedge demonstrates steep eastward-dipping reflections, which suggests that it  
315 represents a sediment slump originating on the inner-trench slope. Trench fill is thought to be  
316 dominated by undeformed forearc-derived sediment and sediment from the subducting plate,  
317 particularly in the vicinity of the sediment-filled LRSC flexural moat (Ballance *et al.*, 1989; von Huene  
318 & Ranero, 2003). Although the presence of a slump indicates that forearc-derived sediment accounts  
319 for some of the fill of the trench along this profile, there is no apparent evidence for other mechanisms  
320 of trench fill.

321 The Tonga and Kermadec trenches are widely considered to be sediment starved, and thus  
322 only exhibit minor sediment fill of <400 m (Karig, 1970; Clift & Vannucchi, 2004; Contreras-Reyes *et al.*,  
323 2011). Profile D indicates a 1 s TWTT thick trench fill that, assuming a sediment velocity of 2000  
324 m s<sup>-1</sup>, equates to ~1 km of sediment. This excess fill may be caused by a greater than expected flux of  
325 forearc-derived material directly into the trench axis (e.g. Ballance *et al.*, 1989), or by increased  
326 sediment transportation along the trench axis (e.g. Völker *et al.*, 2013), which is most likely directed  
327 southwards along the dominant bathymetric gradient, or a combination of both. A similar disparity in  
328 the thickness of trench fill is observed across the intersection of the Juan Fernández Ridge (JFR) with  
329 the central Chile margin (Laurson *et al.*, 2002). The JFR acts as a barrier to the transportation of  
330 sediments north along the central Chile Trench, generating a 2.5 km-thick sediment accumulation  
331 south of the intersection whilst leaving an ~200 m-thick deposit to the north (von Huene *et al.*, 1997;  
332 Laurson *et al.*, 2002). Although the variation in trench-fill across the ridge-trench collision zone is  
333 considerably smaller across the LRSC, trench shallowing of up to 4.5 km around this intersection (see  
334 Fig. 3e) most likely prevents significant sediment transportation between the Tonga and Kermadec  
335 Trenches through a similar mechanism. The vertical succession of bowl-shaped reflections close to the  
336 overriding plate along Profile D suggests that a deep-water channel, ~2 km wide, existed along the  
337 trench that was capable of redistributing sediments, including volcanoclastic material from the LRSC  
338 flexural moat. The presence of such a channel-forming and thus erosive bottom current could also  
339 explain the absence of other features, such as older slumps, in the trench. Despite this, channel  
340 structures are not well defined in the swath bathymetry data collected along the Kermadec trench (Fig.  
341 3e). Channels are, though, observed in a number of trenches around the Pacific (e.g. Lewis, 1994;  
342 Völker *et al.*, 2013), although commonly at shallower depths than the Kermadec trench, which  
343 suggests that their apparent absence here is most likely a result of the complex seabed geometry and  
344 reduced resolution of the bathymetry at depth.

345

#### 346 4.4 Lower-trench slope

347 Despite being imaged for 20 km of Profile D, the structure of the lower-trench slope is poorly resolved  
348 (Fig. 4). Minimal sediment cover ( $<0.1$  s TWTT) causes the bathymetry of the slope to roughly mirror  
349 the irregular surface of the basement (as seen in Karig, 1970). The lack of observed sediments, relative  
350 to the substantial infill of the trench, is most likely the result of the  $\sim 10^\circ$  gradient that encourages  
351 sediment to cascade down the slope and into the trench. Although a frontal prism may be expected at  
352 this convergent margin because of the abundant forearc-derived sediments (von Huene *et al.*, 2004),  
353 the steep angle of slope and lack of actual velocity constraint prevents imaging.

354 The basement of the lower-trench slope is thought to be highly deformed (Karig, 1970;  
355 Dickinson & Seely, 1979). The proposed extensive fracturing of this region, inferred from reduced  
356 seismic wave velocities through the inner trench slope of the Tonga forearc, supports this hypothesis  
357 (Contreras-Reyes *et al.*, 2011). Although a lack of observable faults and offsets along Profile D itself  
358 prevents any definitive conclusions being drawn on the Kermadec lower-trench slope structure, the  
359 irregular surface geometry and steeply dipping nature of the slope along the entire Kermadec forearc  
360 alone suggests that it has been highly deformed (Figs 4b & d).

361

#### 362 4.5 Mid-trench slope

363 Major faulting of the seabed and a significant reduction in bathymetric gradient  $\sim 30$  km west of the  
364 trench, delimit the region where the lower- and mid-trench slopes merge (Fig. 4d). Along Profile D,  
365 the mid-trench slope is dominated by an  $\sim 25$  km wide terrace. This plateau is the surface expression of  
366 a sedimentary wedge that increases in thickness to the east (up to  $\sim 2$  s TWTT), and is bounded by a  
367 750 m-offset, trenchward-dipping normal fault  $\sim 80$  km along the profile (Fig. 4b). High acoustic  
368 backscatter amplitudes along the fault, relative to those from the plateau, suggest that this is the most  
369 recently formed of many large-offset ( $\sim 0.5$  s TWTT) and basement-cutting normal faults observed in  
370 the MCS data (Fig. 4b). Across this fault, the seabed is downthrown to the east; however, where this  
371 fault intersects with the crust, the basement reflector exhibits downthrow to the west. The disparity  
372 between the seabed and basement structure around this fault suggests slip reversal along an older fault,  
373 which is further supported by the divergence of reflectors with proximity to the fault in the lower part  
374 of the sedimentary wedge. This fault reversal, along with older faults that created the uplifted  
375 basement block observed beneath the sediment wedge to the west, suggests that faulting is migrating  
376 eastward across the mid-trench slope. The prevalence of these basement-cutting and apparently  
377 migrating normal faults are facilitating the gradual collapse of the lower- and mid-trench slopes into  
378 the trench, which is evidence that the model of subduction erosion proposed by von Huene *et al.*  
379 (2004) may be occurring here.

380 Significant extension and basin rotation are observed at ODP site 841 and in the MCS data  
381 collected on the Tonga mid-trench slope, near the present day LRSC collision zone (Parson *et al.*,  
382 1992; Clift *et al.*, 1994; Stratford *et al.*, 2014). Clift & MacLeod (1999) use varying rates of  
383 subsidence and tilting to infer that the majority of subduction erosion at this location can be attributed

384 to LRSC subduction. Pervasive, but minor, extensional faulting of the mid-slope plateau is observed in  
385 both the MCS and Parasound data (Figs. 4b and 4a inset respectively), and appears to be in response to  
386 the slight arcward rotation of the eastern end of the wedge following recent fault activation.

387 In contrast to the region proximal to the LRSC (e.g. Clift *et al.*, 1994), the slight extension and  
388 negligible rotation observed along Profile D is evidence of the temporally consistent tectonic erosion  
389 caused by the subduction of background Pacific crust at  $\sim 28^\circ\text{S}$ . Clift & MacLeod (1999) calculate that  
390  $<1.5 \text{ km Myr}^{-1}$  of frontal tectonic erosion occurs along the Tonga-Kermadec subduction system during  
391 this steady-state period. The  $>100 \text{ km}$ -long arcuate normal fault, observed in the swath bathymetry and  
392 backscatter data acquired around Profile D, is similar to and as well defined as a similar structure over  
393  $250 \text{ km}$  further south. To the north of the background subduction zone, the mid-trench slope  
394 extensional features are shorter, less well defined, and thus appear to be more deformed. Subduction of  
395 seamounts, as Ballance *et al.* (1989) suggest, is most likely to have caused these north-south lateral  
396 variations in the characteristics of the deformation of the inner-trench slope.

397 The steep trenchward dip of the basement beneath the mid-trench plateau results in the  
398 sedimentary wedge thinning before abruptly transitioning  $\sim 70 \text{ km}$  west of the trench into the flanks of  
399 a forearc structural high. The across-slope MCS data indicate that a series of basement-cutting normal  
400 faults are overlain by  $<1 \text{ s}$  TWTT of poorly resolved sedimentary units (Fig. 4b). This slope is clearly  
401 defined as a region of high amplitude backscatter and steep slope angles of  $\sim 6^\circ$  (Figs 4d and 4d inset),  
402 which suggest that older sediments have been exposed as a result of a fault-generated gradient and the  
403 subsequent dominance of an erosive regime. Similar backscatter amplitudes, basement faulting and  
404 internal deformation of sedimentary deposits are associated with the juxtaposing forearc structural  
405 high that is uplifted relative to the mid-trench slope and the eastern extent of the upper-trench slope  
406 (Figs 4b & 5b). Whether this feature is caused by active uplift of the structural high or subsidence of  
407 the surrounding trench slopes, its presence suggests that the crust here is more structurally robust than  
408 in surrounding areas of the forearc.

409 Characteristically similar to the upper-trench slope of the Tonga forearc, the eastern slope of  
410 the structural high is observed for over  $2000 \text{ km}$  to the north of Profile D in a number of seismic  
411 reflection and refraction surveys (e.g. Karig, 1970; Lonsdale, 1986; Contreras-Reyes *et al.*, 2011; and  
412 Stratford *et al.*, 2014), swath and global bathymetry data (Figs 4c & 5c), and in backscatter profiles  
413 (e.g. MacLeod & Lothian, 1994). Contreras-Reyes *et al.* (2011) propose that this slope is a scarp; a  
414 surface representation of a crustal-scale, trenchward-dipping listric fault defined by a zone of low  
415 seismic velocity in the overriding plate. Although Profile D demonstrates that this slope is undergoing  
416 extension, there is no direct evidence of a listric fault causing the collapse of the mid-trench slope. The  
417 forearc structural high on Profile D, which is bathymetrically uplifted relative to the trench slopes and  
418 forearc basin, terminates and remains absent from the bathymetry data beyond  $\sim 10 \text{ km}$  south of Profile  
419 D. To the north of the profile, this bathymetric rise merges with the elevated forearc basin of the  
420 Tonga Platform. Although differences in forearc structure may be expected between regions that are  
421 subjected to varying rates of subduction erosion (e.g. Clift & Vannucchi, 2004; von Huene & Scholl,

422 1991), the forearc high is observed for over 250 km to the south of the current LRSC collision zone  
423 (Figs 4 & 5). The mid-trench slope scarp is significantly less prominent south of the LRSC collision,  
424 as adjacent basins are vertically offset by up to 1.5 km south of  $\sim 26^{\circ}\text{S}$  compared to consistent offsets  
425 of  $\sim 3$  km to the north (MacLeod & Lothian, 1994; Lonsdale, 1986; Clift *et al.*, 1998; Contreras-Reyes  
426 *et al.*, 2011). Such substantial discrepancies in the vertical offset along this scarp suggest that the  
427 forces involved in generating this feature have either been on-going for a longer period of time, or are  
428 of a much greater magnitude, north of the LRSC collision. The presence of this mid-trench slope and  
429 structural high, traversing  $\sim 100$  km into the background region of the Kermadec subduction system  
430 despite being less prominent, suggests a link to an underlying forearc structural and deformational  
431 trend, or to the lateral propagation of forearc uplift caused by LRSC indentation.

432

#### 433 *4.6 Upper-trench slope*

434 The upper-trench slope gently rises from the western edge of the forearc structural high to the  
435 Kermadec arc (Fig. 5). Thick sedimentary successions of up to 2 s TWTT, which are divided into two  
436 units by a strong reflection event (located along the pre- and post-hiatus seismostratigraphic boundary  
437 in Fig. 5b), comprise the fill of a forearc basin on the upper-trench slope. The high amplitude  
438 reflection event, which is more prominent than the reflection event associated with the top of the  
439 basement (Fig. 5b – McDougall, 1994), is observed consistently along the Kermadec subduction  
440 system (e.g. Karig 1970; Gillies & Davey, 1986). Parson *et al.* (1992) and Clift *et al.* (1994) record a  
441 depositional hiatus from 32 Ma to 16 Ma that could have enabled the consolidation and diagenesis of  
442 sediments across the forearc and thus, by establishing a density contrast with subsequently deposited  
443 sediments, be capable of generating the observed high-amplitude reflection event. While other causes  
444 of this contrast are plausible, none are observed in the borehole data to an extent that could have  
445 generated the amplitude of this reflection.

446 Reflections from the upper-trench slope are rarely observed for more than 10 km along-profile,  
447 but do show onlap onto the basement and older parts of the sedimentary succession in places. These  
448 observations suggest that sediments on the slope were deposited by temporally distinct events that  
449 originated higher up the forearc (Fig. 5b). Parasound data, which effectively image the shallow  
450 subsurface where the MCS profile only images transparent or chaotic units on the upper-trench slope  
451 along Profile D, and swath bathymetry data indicate the presence of migrating sediment waves on the  
452 forearc basin (Fig. 5a insets). Gillies & Davey (1986) propose that gravity dominated flows initiated  
453 on the forearc high deposit volcanoclastic material as turbidites along the upper-trench slope further  
454 south. Although no sediment cores are available for the Kermadec upper-trench slope, ODP hole 840  
455 confirms the dominance of turbidite deposits on the Tonga forearc to the north (Parson *et al.*, 1992;  
456 Clift, 1994; Clift *et al.*, 1994). The lack of boreholes and cores from the Kermadec upper-trench slope,  
457 and the ambiguity of whether migrating waves observed in Parasound data are formed by down-slope  
458 (turbidite) or along-slope (contourite) flows (Damuth, 1979; Damuth, 1980; Flood, 1980), results in an

459 inconclusive interpretation. However, the migrating waves are evidence of prevalent underwater  
460 currents and significant sediment reworking in the Kermadec forearc basin.

461 Although laterally variable, reflectors on the forearc high are broadly similar (Fig. 5a). They  
462 are concordant with the concave-up structure of the forearc crust, exhibiting dominant dip in the  
463 direction of the trench (Karig, 1970). Dip angle increases with depth through the succession and  
464 suggests that the sediments, which begin to deposit as the gradient of the slope reduces, have been  
465 progressively rotated trenchward since their emplacement (Clift *et al.*, 1994). These tilted sequences  
466 are only present within the westernmost 30 km of the upper trench slope and are particularly  
467 prominent over the region of faulted basement immediately east of the Kermadec arc. Thus, uplift of  
468 the arc relative to the adjacent slopes, rather than the trenchward rotation of the entire forearc, appears  
469 to be the primary mechanism for the adjustment of sediment dip.

470 The upper-trench slope bathymetry along Profile D resembles that observed for almost 200  
471 km to the south (Fig. 5c) and that described by Karig (1970). As such, it is clear that the upper-trench  
472 slope and associated forearc basin along Profile D can be considered as the background structure and,  
473 thus, is undeformed by LRSC collision. Swath data for the region up to 30 km to the north indicates  
474 that the forearc basin structure progressively changes; decreasing in water depth to more closely  
475 reflect the Tonga Ridge geometry (e.g. Contreras-Reyes *et al.*, 2011; Stratford *et al.*, 2014).  
476 Deformation of the forearc in this region is constrained to ~50 km closer to present-day indentation of  
477 the LRSC than was observed in the mid-trench slope. This either suggests that the influence of the  
478 LRSC collision on the different structural blocks varies laterally, or supports the hypothesis that a pre-  
479 existing structural feature may be influencing forearc deformation regardless of the effects of the  
480 LRSC subduction.

481

#### 482 4.7 Kermadec arc

483 The Kermadec arc corresponds to the shallowest part of the Kermadec trench-forearc-backarc system  
484 at 1.5 s TWTT water depth (~1100 m – Fig. 6). Sediments overlying arc basement are poorly resolved  
485 by the MCS data, with the only observable reflection events located on the slope to the east of the  
486 ridge (represented by line drawings of the Kermadec arc sediments in Figs 5b & 6b). These  
487 sedimentary reflectors terminate against the seabed and are discordant with the westernmost  
488 trenchward-dipping units of the upper-trench slope. Strong bottom currents that transport material  
489 along the strike of the ridge may have deposited these westward-dipping sediments and caused their  
490 subsequent erosion. This suggests that the depositional and erosive regimes across the Kermadec arc  
491 are laterally and temporally variable (e.g. Gillies & Davey, 1986).

492 Sediments on the backarc slope onlap against the ~1.3 s TWTT offset normal fault that bounds  
493 the western edge of the Kermadec arc (see Fig. 6b). There is a set of small normal faults (each being  
494 0.1 - 0.2 s TWTT in offset), antithetic to the main fault, which enables the thickness of the sediment  
495 deposits to increase with proximity to the major offset. The sedimentary reflections at the base of the  
496 fault are much less pronounced which indicates that they may be more deformed than those at the top.

497 Together, these observations imply that this major extensional fault has progressively developed  
498 following the initiation of deposition in the region.

499 Uplift or reduced subsidence of the arc, relative to both the upper-trench slope and the backarc,  
500 suggests that the Kermadec arc is underlain by relatively thick, buoyant crust. This structurally high  
501 region may be underlain by a thick low velocity basement, such as that observed ~270 km north of  
502 Profile D beneath the Tonga arc (Stratford *et al.*, 2014). Similar sub-arc basement structure is to be  
503 expected of the Tonga and Kermadec arcs, as the inception of present-day volcanic activity is thought  
504 to have occurred simultaneously along both arcs in response to minor changes in plate motion between  
505 28 and 24 Ma (Lonsdale, 1988; Ballance *et al.*, 1999).

506

#### 507 *4.8 Backarc slope*

508 In the backarc region west of the Kermadec arc, the seabed begins to increase in depth. Sediments are  
509 on average ~0.6 s TWTT thick, and the basement reflector remains roughly concordant with the  
510 seabed (Fig. 6b). A perched basin, observed in both the MCS and swath bathymetry data, lies between  
511 10 and 20 km west of the forearc high. This basin terminates to the west against a large (>0.5 s TWTT  
512 offset) eastward-dipping normal fault that crosscuts the basement and pre-existing sediments. At the  
513 eastern end of the perched basin, lower resolution imaging of the basement results in the inference of a  
514 broad rollover anticlinal structure, which most likely caused the radial normal faults (<0.05 s TWTT  
515 offset) observed in the overlying sediments.

516 Following the generation of the main eastward-dipping fault, infill of this perched basin  
517 reaches 0.4 s TWTT thick (Figs 6a & b). Onlap of both the pre-existing and infill sediments against  
518 this major offset suggests continual displacement, and thus reactivation of the fault. Two antithetic  
519 normal faults, which appear to cause a clockwise rotation of the basement and overlying sediments,  
520 further divide the basin infill and surface, and also indicate recent activation. Smaller-scale faults  
521 (<0.01 s TWTT offset) are evident in the Parasound data and accommodate the extensional stress field  
522 that this rotation generates (Fig. 6a inset). The Parasound profile through the basin also indicates that  
523 infill has occurred in a series of fault-dependent stages, with deposition effectively working to remove  
524 any bathymetric variations.

525 The many scales and prevalence of normal faulting observed west of the Kermadec arc  
526 indicate that this region is being continually extended. These extensional forces may be associated  
527 with extension of the backarc (Delteil *et al.*, 2002) or the oblique subduction angle of the Pacific plate  
528 and LRSC (Pelletier & Louat, 1989; Bonnardot *et al.*, 2007). Although the active centre of the backarc  
529 rift is located >150 km west of the Kermadec arc at this latitude, and is thus unlikely to be inducing  
530 any measurable extension at present, the opening of the Havre Trough ~5 Ma most likely reactivated  
531 existing faults over a broad region (Delteil *et al.*, 2002). Pelletier & Louat (1989) and Bonnardot *et al.*  
532 (2002) note the focal mechanisms of local shallow (<70 km) seismicity that indicate trench-  
533 perpendicular extension, just north of the backarc along Profile D. Despite swath bathymetry data  
534 being sparse for ~50 km south and north of the profile, it is expected that the observed trench-parallel

535 extension is present throughout this region. In comparison, swath bathymetry data further north in the  
536 Tonga arc indicates a series of left-stepping extensional basins (Pelletier & Louat, 1989). These most  
537 likely formed in response to the general extension of the backarc, and have since been pulled apart by  
538 the trench-parallel, strike-slip motion induced by oblique subduction (Delteil *et al.*, 2002; Bonnardot *et*  
539 *al.*, 2007).

540

#### 541 *4.9 Summary of the structural evolution of the Kermadec forearc*

542 Since the initiation of Pacific plate subduction in the middle Eocene, the sedimentary and structural  
543 configuration of the Kermadec forearc has evolved into the system present today. Although Profile D  
544 only images a two-dimensional transect through this complex system, a detailed analysis of the  
545 observed sedimentary units, and their relationships with different structures, enables the evolution of  
546 the forearc to be interpreted. The lack of borehole data in the region prevents the use of date  
547 constraints in understanding this evolution; however, distinct stages of forearc development can be  
548 considered relative to one another to gain a greater insight into major structural changes. Fig. 7  
549 summarises the structural and stratigraphic evolution of the Kermadec forearc along Profile D in four  
550 stages based on previous studies and the interpretation of the MCS and swath bathymetry data  
551 presented in this paper.

552 As subduction initiated along the Tonga-Kermadec trench ~44 Ma, the forearc raised by ~1  
553 km and the trench depressed to its current depth (Parson *et al.*, 1992; Bloomer *et al.*, 1995). After the  
554 initiation of subduction, the forearc evolved through the following stages (see Fig. 7):

555 Stage 1 -

- 556 • Uplift of the Kermadec arc begins (Ballance *et al.*, 1989).
- 557 • Volcanic material is generated along the arc and distributed to the surrounding basins (Clift,  
558 1994).
- 559 • The forearc and backarc basins subside relative to the Kermadec arc.
- 560 • Subduction causes basal subduction erosion and subsequent forearc extension (e.g. von Huene  
561 *et al.*, 2004), promoting fracturing and faulting of the lower- and mid-trench slopes  
562 (Contreras-Reyes *et al.*, 2011).

563 Stage 2 -

- 564 • The backarc slope continues to be downthrown relative to the arc enabling further  
565 sedimentation.
- 566 • Volcaniclastic material accumulates on the trench slope-basins before the onset of a  
567 depositional hiatus from ~32 Ma (Clift *et al.*, 1994).
- 568 • The active landward-dipping normal fault of the mid-trench slope migrates eastward (to fault  
569 1 – Fig. 7), as extension of the forearc slopes continues.
- 570 • Extension of the mid- and upper-trench slopes causes them to subside; the region between  
571 these basins is more structurally robust, and is therefore effectively uplifted.

572 Stage 3 -

- 573 • Extension of the backarc, possibly related to opening of the Havre Trough ~5 Ma (Delteil *et al.*, 2002), produces a seaward normal fault and a perched basin west of the Kermadec arc.
- 574
- 575 • Volcaniclastic material continues to be generated and deposited on the trench slopes from ~16
- 576 Ma (Clift *et al.*, 1994) until ~5 Ma (Delteil *et al.*, 2002).
- 577 • Extension and subsidence of the mid- and upper- trench slopes increases along pre-existing
- 578 faults, e.g. fault 1, and new faults around the forearc structural high.

579 Stage 4 (Present day) -

- 580 • The backarc perched basin begins to be infilled by volcaniclastic material.
- 581 • Deposition of sediments on the upper-trench slope resumes following a period of erosion.
- 582 • Deposits on the forearc structural high are eroded and deposited on the mid-trench slope basin.
- 583 • A reversal in the offset across fault 1 (Fig. 7) and the eastward migration of the active
- 584 landward-dipping fault, to fault 2 (Fig. 7), on the mid-trench slope generates a new basin.

585

## 586 **5 REGIONAL CHANGES IN FOREARC STRUCTURE**

587 The trench-parallel variations in the structural units of the Kermadec trench-forearc-backarc system  
 588 are inherently related and, as such, form coherent blocks observable in regional scale bathymetry and  
 589 satellite-derived free-air gravity anomaly maps (Figs 8a & b respectively – Sandwell & Smith, 2009).  
 590 Perhaps the biggest influence on the development of these blocks is the structure and erosive nature of  
 591 the down-going plate, and the mechanical strength of the overriding plate (von Huene & Scholl, 1991;  
 592 Clift & Vannucchi, 2004; von Huene *et al.*, 2004). Fig. 8a shows that the bathymetry (upper surface)  
 593 of the Pacific oceanic plate is generally smooth, except where the LRSC seamounts protrude up to 3  
 594 km from the seabed (Watts *et al.*, 1988) and in the vicinity of the Tonga-Kermadec trench, where the  
 595 plate bends and is faulted prior to subduction (Lonsdale, 1986; Aubouin, 1989). Although the flexural  
 596 moat surrounding the LRSC is not apparent in the bathymetry data, the free-air gravity anomaly map  
 597 indicates a region of up to 30 mGal lower anomaly amplitude relative to the background oceanic plate  
 598 surrounding the seamount chain (Fig. 8b). This >100 km wide region corresponds to the lateral extent  
 599 of the magma-intruded crust, deeper crust-mantle boundary, and up to 1.6 km thick sediment-filled  
 600 moat constrained by wide-angle seismic refraction data (Contreras-Reyes *et al.*, 2010). The southern  
 601 boundary of this loaded region of oceanic lithosphere coincides with shallowing of the Kermadec  
 602 trench ~150 km to the south of the LRSC collision (Fig. 3c). The free-air gravity anomaly also  
 603 highlights the presence of the Osbourn spreading centre (OSC in Fig. 8a & b) as an east-west trending  
 604 linear feature just north of the LRSC collision zone at ~26°S (Billen & Stock, 2000).

605 Comparison of a series of trench-forearc-backarc profiles (Profiles 1-5 – Fig. 8) extracted from  
 606 the bathymetry and free-air gravity anomaly maps (Figs 8a & b respectively) clearly shows the along-  
 607 strike extent of the major structural units of the Tonga-Kermadec subduction system. A 200 mGal  
 608 negative anomaly region immediately west of the Tonga-Kermadec trench approximately defines the  
 609 lower- and mid-trench slopes of their forearcs, except in the vicinity of the LRSC collision where  
 610 gravity anomaly values only reach -100 mGal. This gravity anomaly across the lower- and mid-trench

611 slopes is most likely caused by the simple bathymetric gradient across the forearc, although the higher  
612 amplitude anomaly present in the LRSC collision zone may be indicative of a currently subducting  
613 seamount (e.g. Timm *et al.*, 2013).

614 Further west, south of 28°S, a gravity anomaly of 0-50 mGal marks the upper-trench slope of  
615 the background Kermadec forearc. The bathymetry of this region displays a marked change in  
616 geometry from being slightly concave in the south (Profiles 1 & 2 – Karig, 1970), through a transition  
617 from Profile 2 (which is coincident with Profile D) to just north of Profile 3, where the forearc is  
618 elevated by ~3 km and convex in shape (associated with a >100 mGal gravity anomaly), typical of the  
619 Tonga forearc basin (Profile 5). With such a clear change in forearc geometry over this region, it  
620 might be inferred that there are significant variations in sedimentary thickness as well as the crustal  
621 structure of the overriding plate (e.g. Ballance *et al.*, 1989). However, the maps and profiles  
622 demonstrate that the relationship between the free-air gravity anomaly and bathymetry vary little  
623 across these zones, except at the southern end of the transitional region between the Kermadec upper-  
624 trench slope and the Tonga Platform. Interestingly, this anomalously high gravity anomaly (>100  
625 mGal) in the transitional zone, which is intersected at its southern extent by Profile 2, coincides with  
626 the inferred structurally robust forearc high observed along Profile D. The positive gravity anomaly  
627 here suggests that the structurally robust crust between the mid- and upper-trench slopes of the  
628 Kermadec forearc is of a higher density than in surrounding regions, and thus may represent a remnant  
629 of the old Eocene arc (Bloomer *et al.*, 1995; Collot & Davy, 1998).

630 The transitional zone between the background forearc (geometrically concave – green region  
631 in Fig. 8c) and highly deformed and elevated Tonga Platform (geometrically convex – red and blue  
632 regions in Fig. 8c) is currently only being directly influenced by background Pacific plate subduction.  
633 Despite the inference of a dense and robust remnant crust underlying the Kermadec structural high,  
634 deformation around this region along Profile D (Profile 2 in Fig. 8) appears to be on-going and of a  
635 greater magnitude than that observed further south. As a result, this transitional feature appears to be  
636 generated by not only an older structural trend, but also by diffuse uplift of the Kermadec forearc  
637 caused by the collision of the LRSC up to 250 km to the north (Parson *et al.*, 1992; Collot & Davy,  
638 1998).

639

## 640 **6 CONCLUSIONS**

641 Despite being unable to image below the top of the basement, the MCS and Parasound data acquired  
642 along Profile D traversing the Kermadec trench and forearc, has enabled the structure and stratigraphy  
643 of the underthrusting (down-going) and overriding plates to be determined. By synthesising this  
644 information with relatively sparse shipboard swath bathymetry datasets and satellite-derived  
645 bathymetry and free-air gravity data, we have been able to relate the observed along-profile  
646 characteristics with trench-parallel variations in background features and underlying subduction  
647 processes. We conclude that:

- 648 1. The subducting plate is characterised by large-offset normal faults, which form horst and  
649 graben structures up to 2 km deep, 15 km across, and >200 km in trench-parallel length. Fault  
650 offsets grow with proximity to the trench, as extensional stresses increase with bending of the  
651 down-going plate.
- 652 2. Although the subducting Pacific plate is poorly sedimented prior to entering the trench (<100  
653 m), trench infill at ~28°S is significantly thicker than expected, exceeding 1 km. This increase  
654 most likely results from increased input of forearc-derived volcanoclastic sediments and the  
655 redistribution of sediments along-trench by an inferred southward-flowing current.
- 656 3. Subduction of the highly-faulted Pacific plate persistently erodes the basal and frontal sections  
657 of the overriding plate, causing continual extension and collapse of the ~70 km wide lower-  
658 and mid-trench slopes. Although this steady-state rate of erosion is thought to be below 1.5  
659 km Myr<sup>-1</sup> (Clift & MacLeod, 1999), the effect is observed in the pervasive normal faulting of  
660 the mid-trench slope as it gradually subsides and collapses into the trench together with the  
661 lower-trench slope.
- 662 4. Striking variations in along-arc bathymetric geometry and the presence of a free-air gravity  
663 anomaly high between the mid- and upper-trench slopes, suggests that a region of higher  
664 density and structurally robust crust sits beneath the forearc structural high.
- 665 5. Proximal to the southern end of the LRSC collision with the Kermadec trench, there is an ~70  
666 km wide concave forearc basin on the upper-trench slope, and the arc forms a single  
667 pronounced ridge. The forearc and backarc slopes are covered by accumulations of locally  
668 derived volcanoclastic sediments, with migrating sediment waves suggesting that reworking of  
669 these deposits by arc-parallel and downslope currents is likely. At least two periods of non-  
670 deposition and erosion are recorded in the MCS data.
- 671 6. Perhaps the most significant observation, however, is the raising and broadening of the forearc  
672 basin immediately north of Profile D. Heading further north, this region develops into the  
673 shallow and wide Tonga Platform over a distance of 250 km, suggesting that an underlying  
674 structural trend may be present, and that LRSC subduction deforms a wider region of the  
675 forearc than its actual footprint on the subducting plate.

676

## 677 **ACKNOWLEDGEMENTS**

678 We would like to thank all those involved in the data acquisition for the *R/V Sonne* cruise SO215,  
679 including the captain, crew and sea-going technicians from the U.K.'s Natural Environment Research  
680 Council (NERC) National Marine Facility Sea Systems and Exploration Electronics Ltd. We are  
681 grateful to the two anonymous reviewers for their thoughtful and helpful comments on this paper. The  
682 MCS data were processed and plotted using Claritas<sup>TM</sup>. All other figures were generated with the  
683 Generic Mapping Tools (Wessel & Smith, 1998). This research was funded by the NERC (grant  
684 reference NE/F004273/1) in collaboration with the *Tonga Thrust* earthquake *Asperity* at *Louisville*  
685 *Ridge* (TOTAL) project (Peirce & Watts, 2011). All data from cruise SO215 are archived at the

686 NERC's British Oceanographic Data Centre (BODC), and the final submitted version of this  
687 manuscript is available through Durham Research Online ([dro.dur.ac.uk](http://dro.dur.ac.uk)).

688 **REFERENCES**

- 689 Aubouin, J., 1989. Some aspects of the tectonics of subduction zones, *Tectonophysics*, **160**, 1-21.
- 690 Ballance, P.F., Scholl, D.W., Vallier, T.L., Stevenson, A.J., Ryan, H. & Herzer, R.H., 1989.  
691 Subduction of a late Cretaceous seamount of the Louisville Ridge at the Tonga Trench; A  
692 model of normal and accelerated tectonic erosion, *Tectonics*, **8**, 953-962.
- 693 Ballance, P.F., Ablaev, A.G., Pushchin, I.K., Pletnev, S.P., Birylyna, M.G., Itaya, T., Follas, H.A. &  
694 Gibson, G.W., 1999. Morphology and history of the Kermadec trench-arc-backarc basin-  
695 remnant arc system at 30 to 32°S: geophysical profile, microfossil and K-Ar data, *Marine*  
696 *Geology*, **159**, 35-62.
- 697 Bevis, M., Taylor, F.W., Schutz, B.E., Recy, J., Isacks, B.L., Hlu, S., Singh, R., Kendrick, E., Stowell,  
698 J., Taylor, B. & Calmant, S., 1995. Geodetic observations of very rapid convergence and  
699 back-arc extension at the Tonga arc, *Nature*, **374**, 249-51.
- 700 Billen, M., & Stock, J., 2000. Morphology and origin of the Osborn Trough. *J. Geophys. Res.*, **105**,  
701 481-489.
- 702 Billen, M., Cowgill, E., Buer, E., 2007. Determination of fault friction from reactivation of abyssal-hill  
703 faults in subduction zones. *Geology*, **35**, 819-822.
- 704 Bloomer, S.H., Taylor, B., MacLeod, C.J., Stern, R.J., Fryer, P., and Johnson, L., 1995. Early arc  
705 volcanism and the ophiolite problem: A perspective from drilling in the western Pacific, *in*  
706 Taylor, B., and Natland, J.H., eds., *Active margins and marginal basins; a synthesis of ocean*  
707 *drilling in the western pacific: American Geophysical Union monograph*, **88**, 1-30.
- 708 Bonnardot, M.-A., Régnier, M., Ruellan, E., Christova, C. & Tric, E., 2007. Seismicity and state of  
709 stress within the overriding plate of the Tonga-Kermadec subduction zone, *Tectonics*, **26**,  
710 TC5017, doi:10.1029/2006TC002044.
- 711 Bouma, A.H., 1962. Sedimentology of some flysch deposits: A graphic approach to facies  
712 interpretation, Elsevier, Amsterdam.
- 713 Brodie, J.W. & Hatherton, T., 1958. The morphology of Kermadec and Hikurangi trenches, *Deep-Sea*  
714 *Research*, **5**, 18-28.
- 715 Burns, R.E., Andrews, J.E. & van der Lingen, G.J., 1973. Site 204 Initial Report, *in* Proceedings of the  
716 Ocean Drilling Program, 21: College Station, Texas, Ocean Drilling Program, 33-56.
- 717 Caldwell, J.G., Haxby, W.F., Karig, D.E. & Turcotte, D.L., 1976. Observations of flexure and the state  
718 of stress in the oceanic lithosphere. *Earth and Planetary Science Letters*, **31**, 239-246.
- 719 Caress, D.W. & Chayes, D.N., 1996. Improved processing of Hydrosweep data on the R/V *Maurice*  
720 *Ewing*, *Marine Geophysical Researches*, **18**, 631-650.
- 721 Castillo, P.R., Lonsdale, P.F., Moran, C.L. & Hawkins, J.W., 2009. Geochemistry of mid-Cretaceous  
722 Pacific crust being subducted along the Tonga-Kermadec Trench: Implications for the  
723 generation of arc lavas, *Lithos*, **112**, 87-102.

- 724 Clift, P.D., 1994. Controls on the sedimentary and subsidence history of an active plate margin: an  
725 example from the Tonga Arc (southwest Pacific), *Proceedings of the Ocean Drilling*  
726 *Program, Scientific results*, **135**, 173-188.
- 727 Clift, P.D. & MacLeod, C.J., 1999. Slow rates of subduction erosion estimated from subsidence and  
728 tilting of the Tonga forearc, *Geology*, **27**, 411-414.
- 729 Clift, P.D. & Vannucchi, P. 2004, Controls on tectonic accretion versus erosion in subduction zones:  
730 Implications for the origin and recycling of the continental crust. *Rev. Geophys.*, **42**, RG2001,  
731 doi:10.1029/2003RG000127.
- 732 Clift, P.D., Bednarz, U., Bøe, R., Rothwell, G., Hodkinson, R.A., Ledbetter, J.K., Pratt, C.E. & Soakai,  
733 S., 1994. Sedimentation on the Tonga forearc related to arc rifting, subduction, erosion, and  
734 ridge collision: A synthesis of results from sites 840 and 841, *Proceedings of the Ocean*  
735 *Drilling Program, Scientific results*, **135**, 843-855.
- 736 Clift, P.D., MacLeod, C.J., Tappin, D.R., Wright, D.J. & Bloomer, S.H., 1998. Tectonic controls on  
737 sedimentation and diagenesis in the Tonga Trench and forearc, southwest Pacific. *Geological*  
738 *Society of America Bulletin*, **110**, 483-496.
- 739 Collot, J.-Y. & Davy., 1998. Forearc structures and tectonic regimes at the oblique subduction zone  
740 between the Hikurangi Plateau and the southern Kermadec margin. *J. Geophys. Res.*, **103**,  
741 623-650.
- 742 Contreras-Reyes, E., Grevenmeyer, I., Watts, A.B., Planert, L., Flueh, E.R. & Peirce, C., 2010. Crustal  
743 intrusion beneath the Louisville hotspot track, *Earth Planet. Sci. Lett.*, **289**, 323-333,  
744 doi:10.1016/j.epsl.2009.11.020.
- 745 Contreras-Reyes, E., Grevenmeyer, I., Watts, A.B., Flueh, E.R., Peirce, C., Moeller, S. & Papenberg, C.,  
746 2011. Deep seismic structure of the Tonga subduction zone: Implications for mantle hydration,  
747 tectonic erosion, and arc magmatism, *J. Geophys. Res.*, **116**, B10103,  
748 doi:10.1029/2011JB008434.
- 749 Damuth, J.E., 1979. Migrating sediment waves created by turbidity currents in the northern South  
750 China Basin. *Geology*, **7**, 520-523.
- 751 Damuth, J.E., 1980. Use of high-frequency (3.5-12 kHz) echograms in the study of near-bottom  
752 sedimentation processes in the deep-sea: A review. *Marine Geology*, **38**, 51-75.
- 753 Davy, B., 1992. The influence of subducting plate buoyancy on subduction of the Hikurang-Chatham  
754 Plateau beneath North Island, New Zealand, in *Geology and Geophysics of Continental*  
755 *Margins*, edited by J.S. Watkins, F. Zhiqiang, and K.J. McMillen, *AAPG Mem.*, **53**, 75-91.
- 756 Davy, B. & Collot, J.-Y., 2000. The Rapuhia Scarp (northern Hikurangi Plateau) – its nature and  
757 subduction effects on the Kermadec Trench, *Tectonophysics*, **328**, 269-295.
- 758 Delteil, J., Ruellan, E., Wright, I. & Matsumoto, T., 2002. Structure and structural development of the  
759 Havre Trough (SW Pacific), *J. Geophys. Res.*, **107**, ETG 7: 1-17 doi:10.1029/2001JB000494.
- 760 Dickinson, W.R. & Seely, D.R., 1979. Structure and stratigraphy of forearc regions, *Amer. Assoc. of*  
761 *Pet. Geol. Bulletin*, **63**, 2-31.

762 Flood, R.D., 1980, Deep-sea sedimentary morphology: Modelling and interpretation of echo-sounding  
763 profiles. *Marine Geology*, **38**, 77-92.

764 Gillies, P.N. & Davey, F.J., 1986. Seismic reflection and refraction studies of the Raukumara forearc  
765 basin, New Zealand, *New Zealand J. of Geol. and Geophys.*, **29**, 391-403.

766 Grevemeyer, I., & Flüh, E., 2008. FS Sonne SO195 Cruise Report: TONGA Thrust earthquake Asperity  
767 at Louisville ridge (TOTAL). pp 101.

768 Grevemeyer, I., Kaul, N., Diaz-Naveas, J. L., Villinger, H. W., Ranero, C. R., & Reichert C., 2005.  
769 Heat flow and bending-related faulting at subduction trenches: Case studies offshore of  
770 Nicaragua and central Chile, *Earth Planet. Sci. Lett.*, **236** (1-2), 238–248,  
771 doi:10.1016/j.epsl.2005.04.048.

772 Habermann, R.E., McCann, W.R. & Perin, B., 1986. Spatial seismicity variations along convergent  
773 plate boundaries, *Geophys. J. R. astr. Soc.*, **85**, 43–68.

774 Hawkins, J.W., Bloomer, S.H., Evans, C.A. & Melchior, J.T., 1984. Evolution of intra-oceanic arc-  
775 trench systems, *Tectonophysics*, **102**, 175-205.

776 Herzer, R.H., Scholl, D.W. & Scientific Staff, 1984. Initial report on 1984 R/V S.P. Lee cruise L3-84-  
777 SP: Tonga Ridge, Lau Ridge, and Lau Basin. *SOPAC Cruise Report No. 93*, pp. 8.

778 von Huene, R. & Scholl, D.W., 1991. Observations at convergent margins concerning sediment  
779 subduction, subduction erosion, and the growth of continental crust. *Reviews of Geophysics*,  
780 **29**, 279-316.

781 von Huene, R. & Ranero, C.R., 2003. Subduction erosion and basal friction along the sediment-  
782 starved convergent margin off Antofagasta, Chile. *J. Geophys. Res.*, **108**, B2 pp 16.

783 von Huene, R., Corvalán, J., Flueh, E.R., Hinz, K., Korstgard, J., Ranero, C.R., Weinrebe, W., & the  
784 CONDOR Scientists, 1997. Tectonic control of the subducting Juan Fernández Ridge on the  
785 Andean margin near Valparaíso, Chile, *Tectonics*, **16**, No. 3, 474-488.

786 von Huene, R., Ranero, C.R. & Vannucchi, P., 2004. Generic model of subduction erosion. *Geology*,  
787 **32**, 913-916.

788 Intergovernmental Oceanographic Commission (IOC), International Hydrographic Organization  
789 (IHO), and British Oceanographic Data Centre (BODC), 2003. "Centenary Edition of the  
790 General Bathymetric Chart of the Oceans Digital Atlas", Published on CDROM on Behalf of  
791 the IOC and the IHO as Part of the GEBCO; BODC, Liverpool.

792 Karig, D.E., 1970. Ridges and basins of the Tonga-Kermadec Island Arc System, *J. Geophys. Res.*, **75**,  
793 239-254.

794 Katz, H.R., 1981. Plate margin transition from oceanic arc-trench to continental system: the  
795 Kermadec-New Zealand example, *Tectonophysics*, **87**, 49-64.

796 Laursen, J., Scholl, D.W. & von Huene, R., 2002. Neotectonic deformation of the central Chile  
797 margin: Deepwater forearc basin formation in response to hot spot ridge and seamount  
798 subduction, *Tectonics*, **21**, No. 5, 1-27.

- 799 Lewis, K. B., 1994. The 1500 km-long Hikurangi Channel: trench-axis channel that escapes its trench,  
800 crosses a plateau, and feeds a fan drift, *Geo-Marine Letters* **14**, 19-28.
- 801 Lonsdale, P., 1986. A multibeam reconnaissance of the Tonga Trench axis and its intersection with the  
802 Louisville guyot chain, *Marine Geophysical Researches*, **8**, 295-327.
- 803 Lonsdale, P., 1988. Geography and History of the Louisville Hotspot Chain in the Southwest Pacific,  
804 *J. Geophys. Res.*, **93**, 3078-3104.
- 805 MacLeod, C.J., 1994. Structure of the outer Tonga forearc at site 841, *Proceedings of the Ocean*  
806 *Drilling Program, Scientific results*, **135**, 313-329.
- 807 MacLeod, C.J. & Lothian, A., 1994. Comparison of GLORIA sidescan sonar and core derived  
808 structural data from Site 841, Tonga Trench, *Proceedings of the Ocean Drilling Program,*  
809 *Scientific results*, **135**, 373-382.
- 810 Maksymowicz, A., Conreras-Reyes, E., Grevemeyer, I. & Flueh, E., 2012. Structure and geodynamics  
811 of the post-collision zone between the Nazca-Antarctic spreading center and South America.  
812 *Earth Planet. Sci. Lett.*, **345-348**, 27-37, doi:dx.doi.org/10.1016/j.epsl.2012/06.023
- 813 Malahoff, A., Feden, R.H. & Fleming, H.S., 1982. Magnetic anomalies and tectonic fabric of marginal  
814 basins north of New Zealand, *J. Geophys. Res.*, **87**, 4109-4125.
- 815 McDougall, I., 1994. Data Report: Dating of rhyolitic glass in the Tongan forearc (hole 841B),  
816 *Proceedings of Ocean Drilling Program, Scientific Results*, **135**, 923-924.
- 817 Parson, L., Hawkins, J. & Allan, J., 1992. Site 840 Initial Report, *in* Proceedings of the Ocean Drilling  
818 Program, 135: College Station, Texas, Ocean Drilling Program, 313-329.
- 819 Peirce, C. & Watts, A.B., 2011. R/V Sonne SO215 Cruise Report, The Louisville Ridge-Tonga Trench  
820 collision: Implications for subduction zone dynamics, *Unpublished*, pp. 76.
- 821 Pelletier, B. & Dupont, J., 1990. Erosion, accretion, back-arc extension and slab length along the  
822 Kermadec subduction zone, Southwest Pacific, *Marine Geology*, **310**, 1657-1664.
- 823 Pelletier, B. & Louat, L., 1989. Seismotectonics and present-day relative plate motions in the Tonga-  
824 Lau and Kermadec-Havre region, *Tectonophysics*, **165**, 237-250.
- 825 Pontoise, B. et al. (1986), La subduction de la ride de Louisville le long de la fosse des Tonga:  
826 premiers resultats de la campagne SEAPSO (Leg V). *C. R. Acad. Sc. Paris*, v. 303, Serie II,  
827 no. 10., p. 911-918.
- 828 Ranero, C.R., Phipps Morgan, J., McIntosh, K. & Reichert, C., 2003. Bending-related faulting and  
829 mantle serpentinization at the Middle America trench. *Nature*, 425, 367-373. Habermann, R.E.,  
830 McCann, W.R. & Perin, B., 1986. Spatial seismicity variations along convergent plate  
831 boundaries, *Geophys. J. R. astr. Soc.*, **85**, 43-68.
- 832 Ranero, C.R., von Huene, R., Weinrebe, W. & Reichert, C., 2006. Tectonic processes along the Chile  
833 Convergent Margin, in *Frontiers in Earth Sciences*, vol. 3, The Andes: Active Subduction  
834 Orogeny, edited by O. Oncken *et al.*, pp. 91-121, Springer, Berlin.

835 Sandwell, D.T., & Smith, W.H.F., 2009. Global marine gravity from retracked Geosat and ERS-1  
836 altimetry: Ridge segmentation versus spreading rate. *J. Geophys. Res.*, **114**, BO1411,  
837 doi:10.1029/2008JB006008.

838 Shreve, R.L. & Cloos, M., 1986. Dynamics of sediment subduction, melange formation, and prism  
839 accretion, *J. Geophys. Res.*, **91 (B10)**, 10229-10245.

840 Stratford, W.A., Peirce, C., Funnell, M.J., Paulatto, M., Watts, A.B., Grevemeyer, I. & Basset, D.,  
841 2014. Louisville Ridge seamount subduction effects on forearc morphology and seismic  
842 structure of the Tonga-Kermadec subduction zone. *Geophys. J. Int.*, in review.

843 Sutherland, R., 1995. The Australia-Pacific boundary and Cenozoic plate motions in the SW Pacific:  
844 Some constraints from Geosat data. *Tectonics*, **14**, 819-831.

845 Timm, C., Bassett, D., Graham, I.J., Leybourne, M.I., de Ronde, C.E.J., Woodhead, J., Layton-  
846 Matthews, D. & Watts, A.B., 2013. Louisville seamount subduction and its implication on  
847 mantle flow beneath the central Tonga-Kermadec arc. *Nature Communications*. **4:1720**,  
848 DOI:10.1038/ncomms2702.

849 Völker, D., Geersen, J., Contreras-Reyes, E. & Reichert, C., 2013. Sedimentary fill of the Chile  
850 Trench (32-46°): volumetric distribution and causal factors. *Journal of the Geological Society,*  
851 *London*. **79**, 723-736.

852 Watts, A.B., Bodine, J.H. & Steckler, M.S., 1980. Observations of flexure and the state of stress in the  
853 oceanic lithosphere. *J. Geophys. Res.*, **85**, 6369-6376.

854 Watts, A.B., Weissel, J.K., Duncan, R.A. & Larson, R.L., 1988. Origin of the Louisville Ridge and its  
855 relationship to the Eltanin Fracture Zone system, *J. Geophys. Res.*, **92**, 3051-3077.

856 Wessel, P. & Smith, W.H.F., 1998. New, improved version of the Generic Mapping Tools released,  
857 *EOS Trans. AGU*, **79**, 579.

858 **FIGURE CAPTIONS**

859

860 *The figures accompanying this manuscript are low resolution to facilitate submission of the*  
861 *manuscript due to their byte size.*

862

863 **Figure 1.** Bathymetry map of the Tonga-Kermadec subduction system. The study area, indicated by  
864 the black box on the inset map, stretches from 22-30°S and 173-178.5°W. The inset map shows that  
865 although the Pacific plate (PP) subducts beneath the Indo-Australian plate (I-AP) along the length of  
866 this subduction zone, the Kermadec trench (KT) is separated from the Tonga and Hikurangi trenches  
867 (TT and HT) by the collision of the Louisville Ridge seamount chain (LRSC) and Hikurangi Plateau  
868 respectively. Profile D (red line) is an MCS transect through the Kermadec trench-forearc system at  
869 ~28°S, located to image the structural and stratigraphic development of the forearc. The study location  
870 map is repeated in Figs 2-6 to indicate the extent of MCS and bathymetry data displayed within each  
871 figure, and to locate each figure within the regional context.

872

873 **Figure 2.** Major structural units of the Tonga-Kermadec trench-forearc system (top) characterised by  
874 (a) the swath bathymetry and (b) MCS data acquired along Profile D. KR is the Kermadec ridge.  
875 Profile D is marked by a red line in (a) and (c). Boxes and numbers indicate the extents of Figs. 3-6 to  
876 aid correlation of specific features within the context of the entire seismic profile. A dashed line  
877 indicates the water column multiple. Offsets along all subsequent seismic sections and bathymetry  
878 maps increase westward and northward from the origin of Profile D, as shown in (a). c) Extent of the  
879 bathymetry and MCS data (black box and red line respectively) displayed in this figure, shown relative  
880 to the study area.

881

882 **Figure 3.** a) Processed seismic section of the subducting Pacific plate and Kermadec trench, with the  
883 inset section highlighting the nature of sedimentary reflections on the down-going plate. Black outline  
884 box indicates the region of MCS data shown in Fig. 3c. b) Interpreted seismic section. Inset key  
885 indicates the different seismostratigraphic units. c) Detailed image of the sediment-filled trench. Note  
886 the reflection geometry varies laterally through the trench fill, from horizontal and planar in the east to  
887 concave-up structures in the west. d) Extent of the bathymetry and MCS data (black box and red line  
888 respectively) displayed in this figure, shown relative to the study area. e) Combined swath and  
889 satellite-derived bathymetry map of the subducting plate and trench around Profile D.

890

891 **Figure 4.** a) Annotated seismic reflection image of the lower and mid-trench slopes of the overriding  
892 Pacific plate. The onset of the water column multiple is indicated by arrows. Dashed red box indicates  
893 the extent of the inset Parasound data. b) Interpretation of the features in a), with inset key to indicate  
894 the different seismostratigraphic units. c) Extent of the bathymetry and MCS data (black box and red  
895 line respectively) displayed in this figure, shown relative to the study area. d) Swath bathymetry map  
896 of the lower- and mid-trench regions, highlighting lateral changes in seabed structure. The zoom-in  
897 box highlights a recently formed fault surface, and the forearc structural high and its flanks, with their  
898 relatively high backscatter amplitudes (lighter regions).

899

900 **Figure 5.** a) Annotated seismic reflection image of the Kermadec forearc structural high, upper-trench  
901 slope and arc. An arrow highlights the onset of the water column multiple on the section. Two  
902 Parasound sections, P-1 and P-2, and a magnified region of swath bathymetry data are inset to indicate  
903 the migrating sediment waves observed in the shallow subsurface. b) Interpreted seismic section. The  
904 different sedimentary seismostratigraphic units indicated in the section and inset key represent  
905 sequences that are separated by depositional hiatuses and erosional surfaces. c) Swath bathymetry map,  
906 centred on the upper-trench slope of the Tonga-Kermadec subduction system, highlights variations  
907 between background and raised forearc structure. d) Extent of the bathymetry and MCS data (black  
908 box and red line respectively) displayed in this figure, shown relative to the study area.

909

910 **Figure 6.** a) Seismic section across the Kermadec arc and slope into the backarc. The water column  
911 multiple is indicated by arrows, and the red-dashed box shows the extent of the inset Parasound data,  
912 which images up to ~75 m of basin infill. Note the apparent lack of reflections above the basement of  
913 the Kermadec arc. b) Annotated interpretation of (a), with inset key indicating the different  
914 seismostratigraphic units displayed. c) Swath bathymetry data along the Kermadec and Tonga arcs. d)  
915 Extent of the bathymetry and MCS data (black box and red line respectively) displayed in this figure,  
916 shown relative to the study area.

917

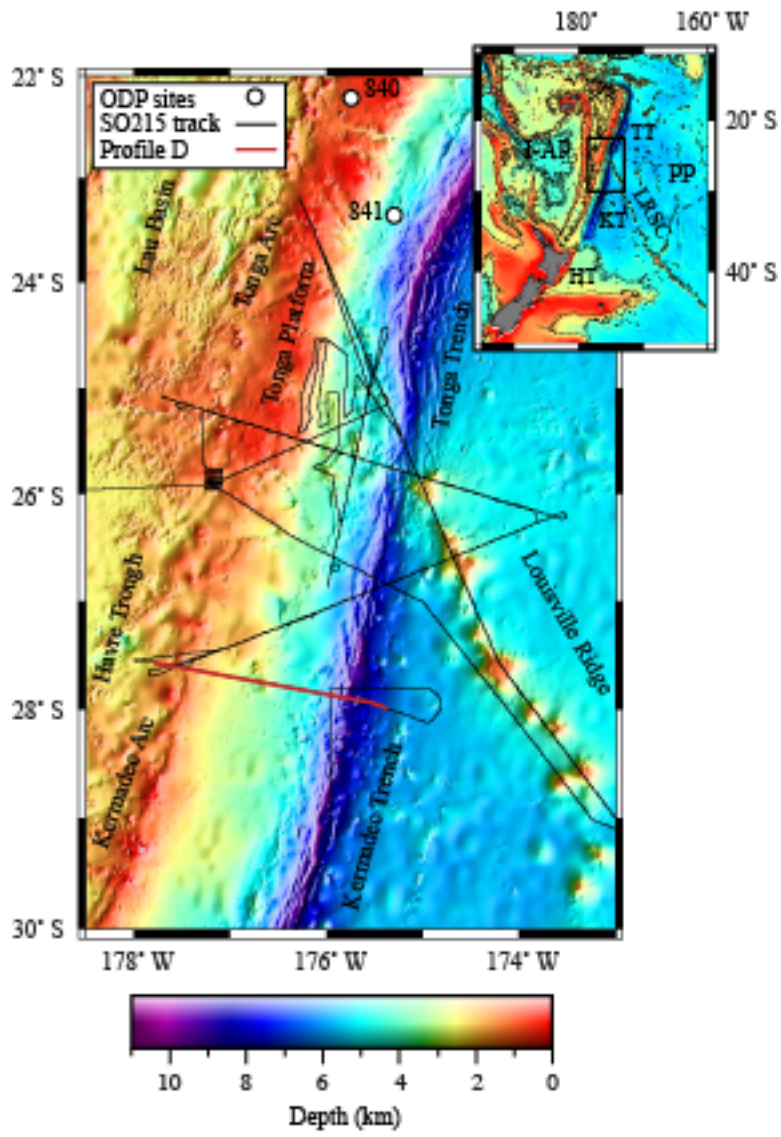
918 **Figure 7.** A series of schematic diagrams representing the proposed evolution of the Kermadec forearc  
919 along Profile D, based on previous studies and the interpretation of the MCS and swath bathymetry  
920 data presented in Figs 3-6. Stages 1-4 define key periods of forearc development, focussing on major  
921 structural and stratigraphic changes, with Stage 4 being a simplified model of the present-day forearc  
922 structure. The different stages are loosely defined spatially and temporally due to a lack of constraint  
923 from borehole data. The background mesh indicates the major forearc structural units: the lower-, mid-,  
924 and upper-trench slopes, the Kermadec ridge (KR), and the backarc.

925

926 **Figure 8.** a) Bathymetry and b) satellite-derived free-air gravity anomaly maps of the Tonga-  
927 Kermadec study region. A dashed black line indicates the location of the Osbourn Spreading Centre  
928 (OSC). Profiles 1-5 were selected to sample the Kermadec forearc, where swath bathymetry data has  
929 been acquired, whilst being separated by a relatively consistent offset. Profile 2 is coincident with  
930 Profile D. The free-air gravity anomaly map highlights the presence of the LRSC and moat on the  
931 subducting plate, and indicates distinct variations between the pre-, current- and post-collision zones.  
932 These different zones are outlined in c) by the green, red and blue boxes respectively. The yellow  
933 region represents the volcanic arc, and the orange cross-hachured box over the pre-collision zone  
934 delimits the region of transitional deformation. To the right of c), profiles of bathymetry (black lines,  
935 with blue lines representing normal Kermadec forearc structure along Profile 1 for comparison) and  
936 the free-air gravity anomaly (blue lines) show the along-forearc changes in structure and deformation.  
937  
938

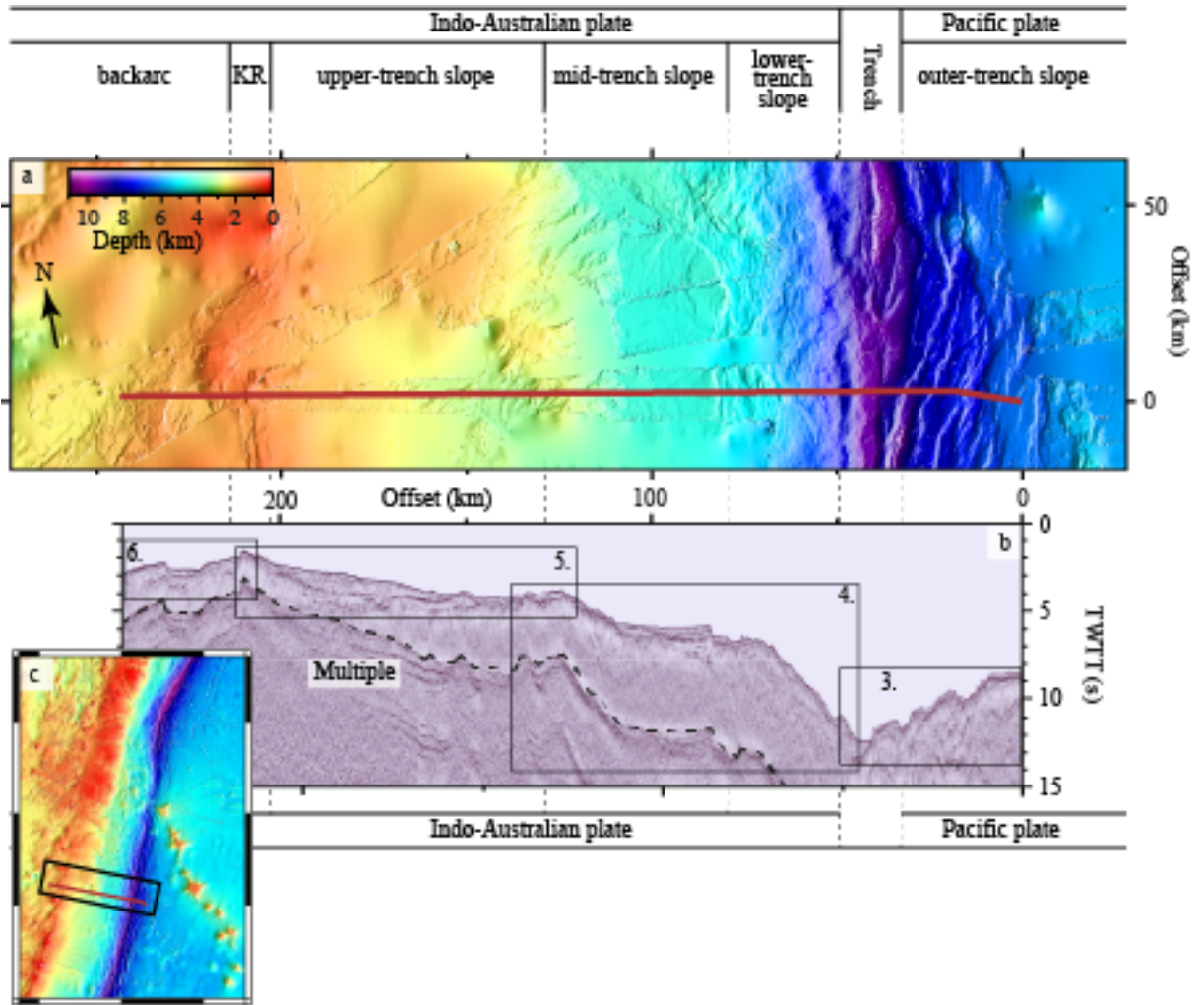
939 **Figure 1**

940



941

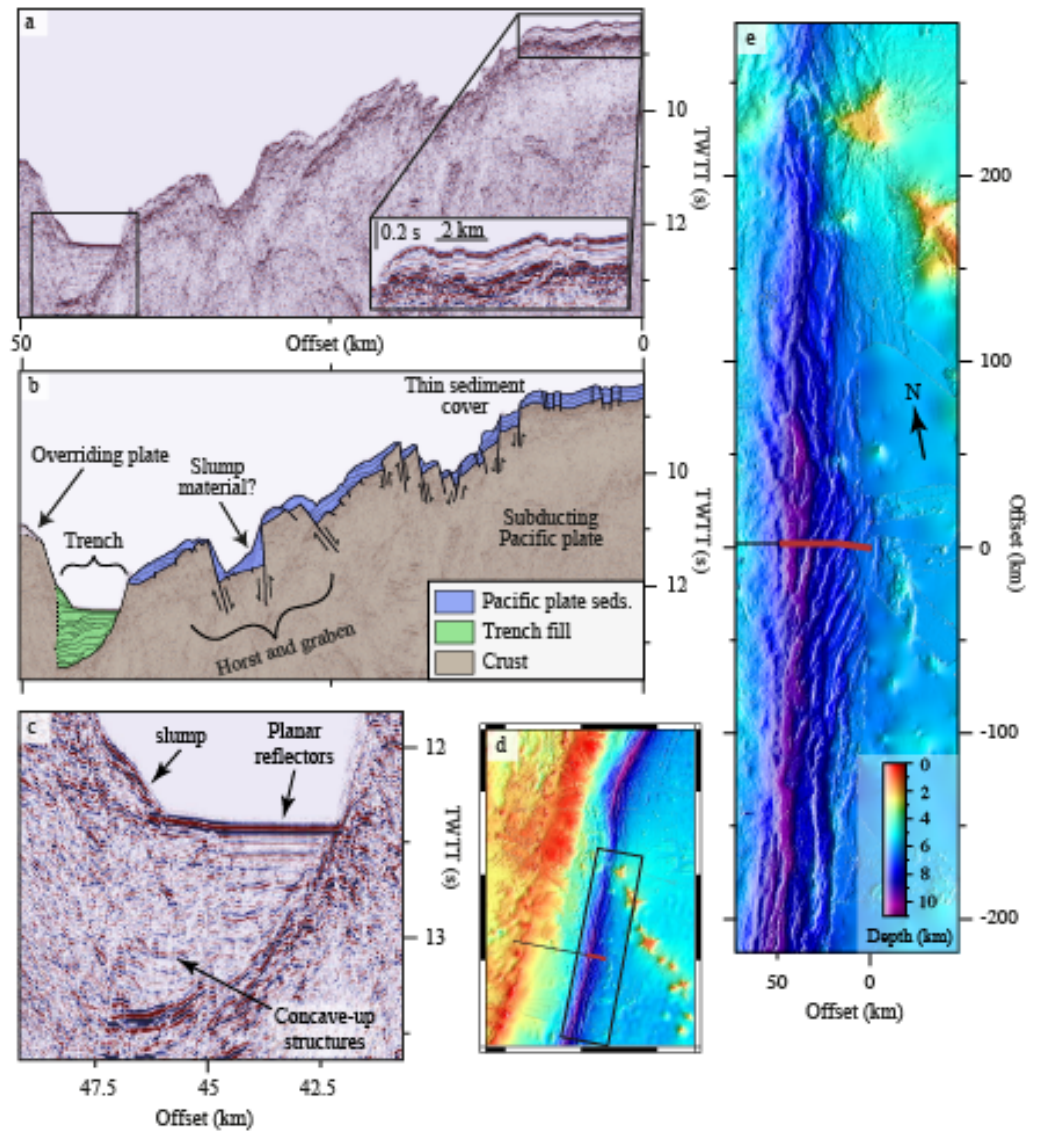
942 **Figure 2**



943

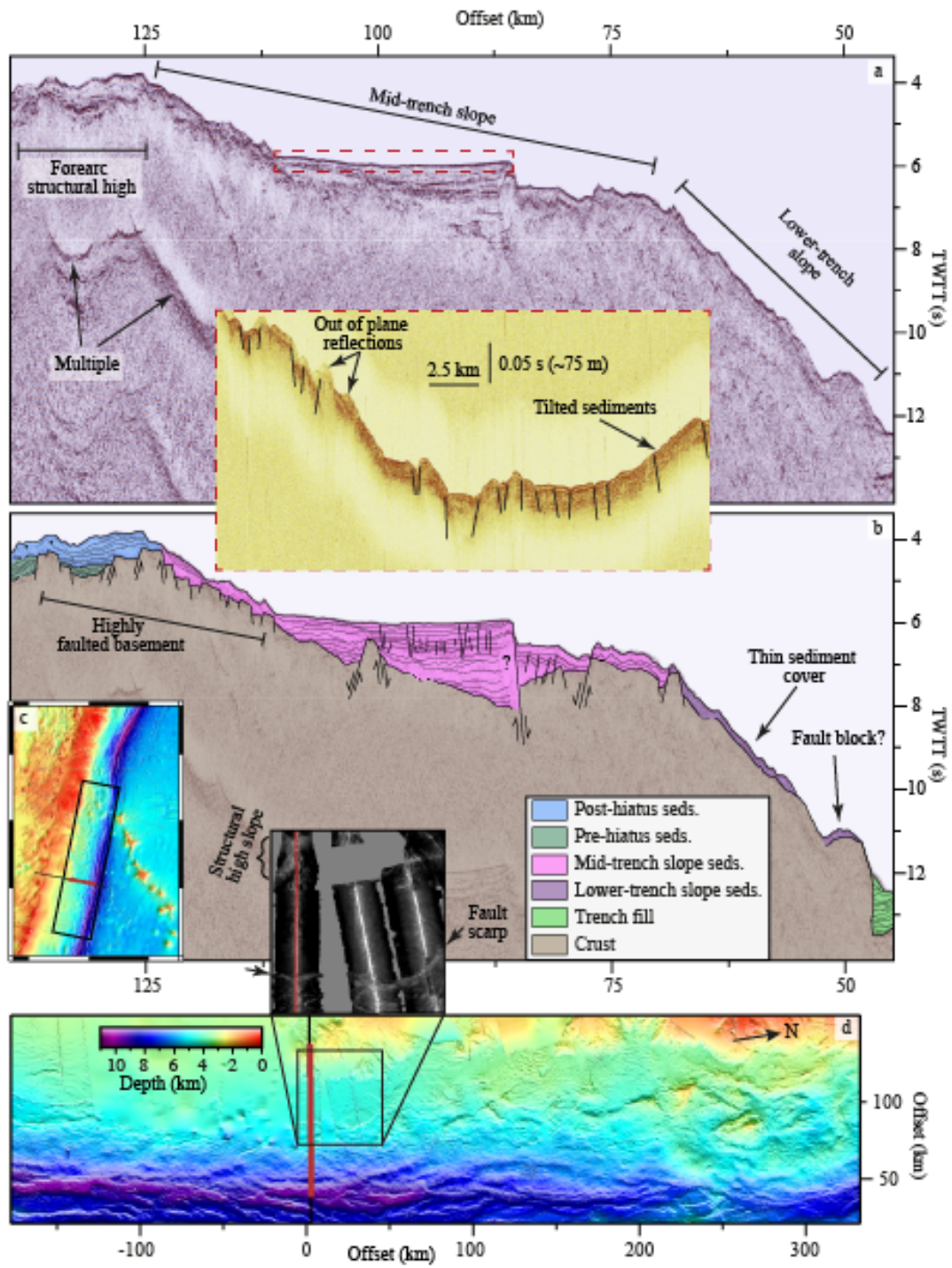
944

945 **Figure 3**  
946



947

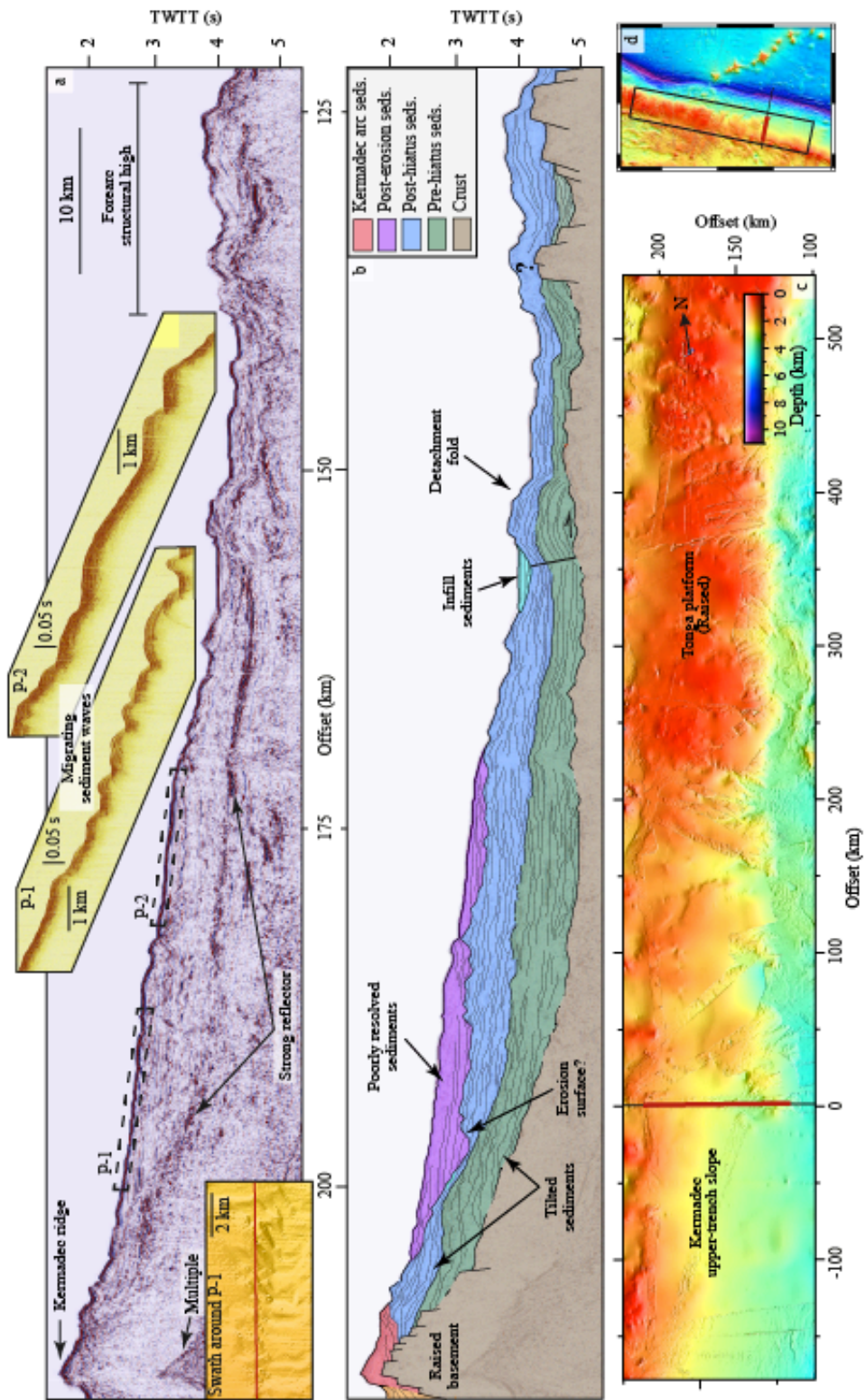
948 Figure 4



949

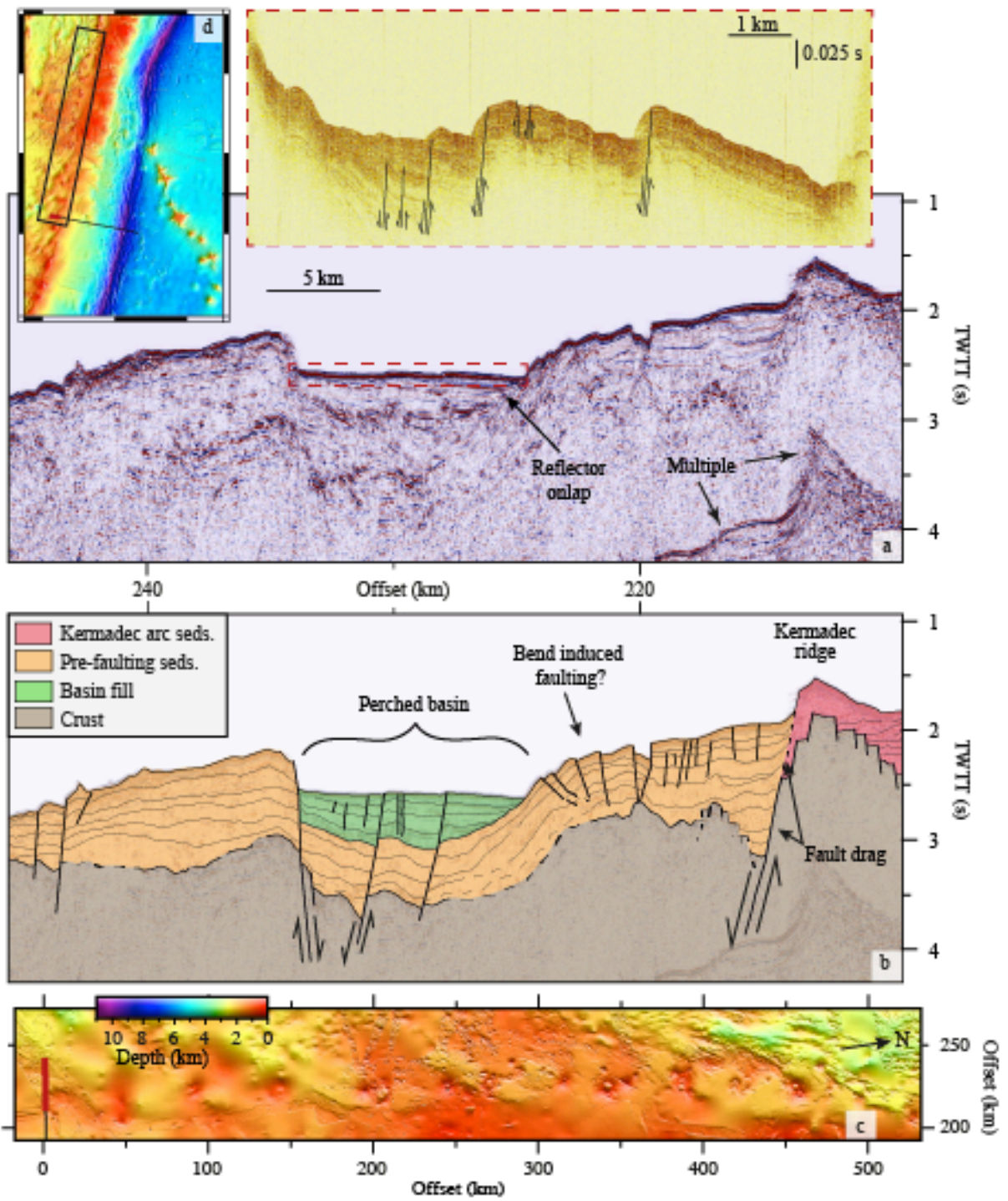
950

951 **Figure 5**  
 952  
 953



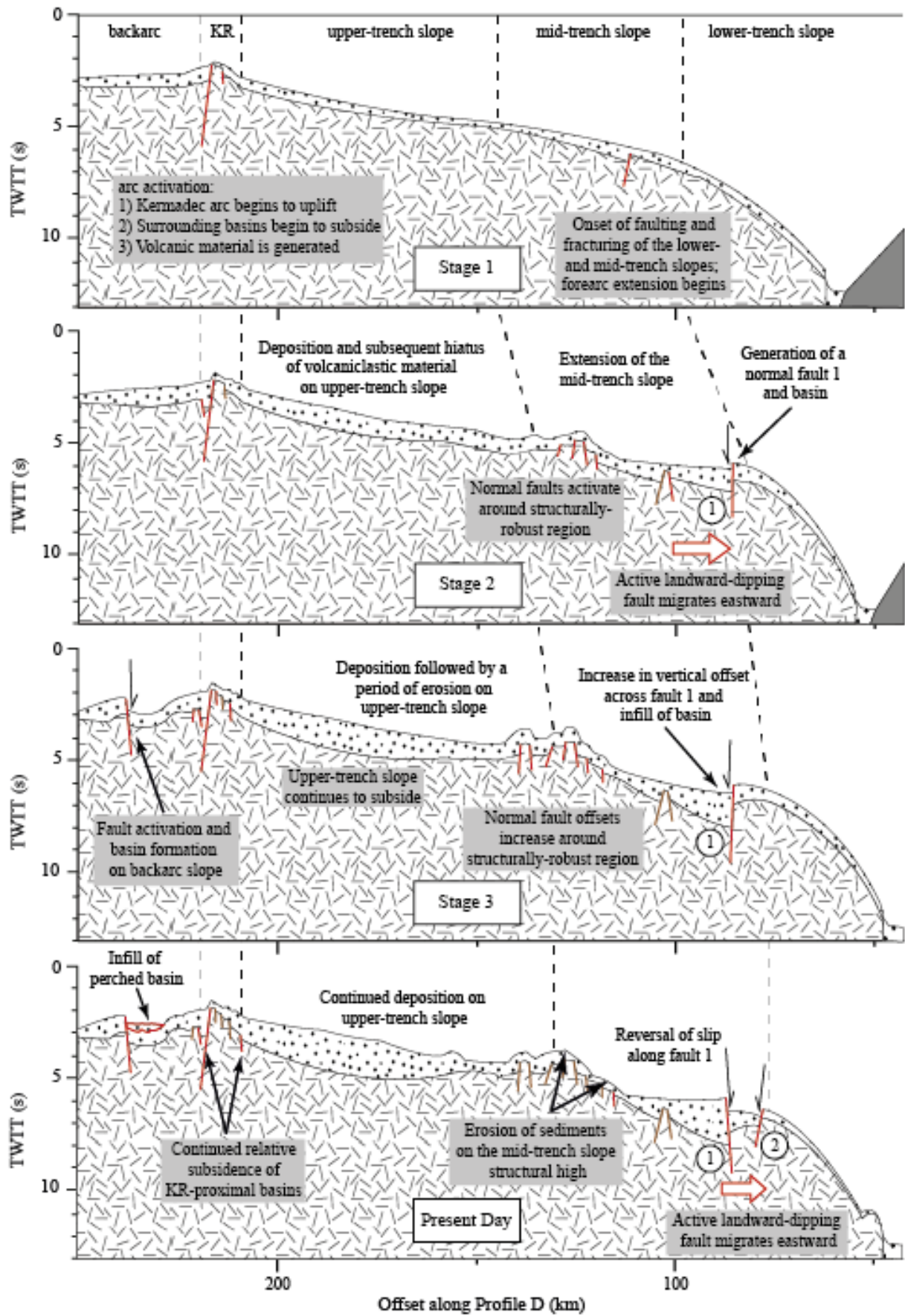
954 Figure 6

955



956

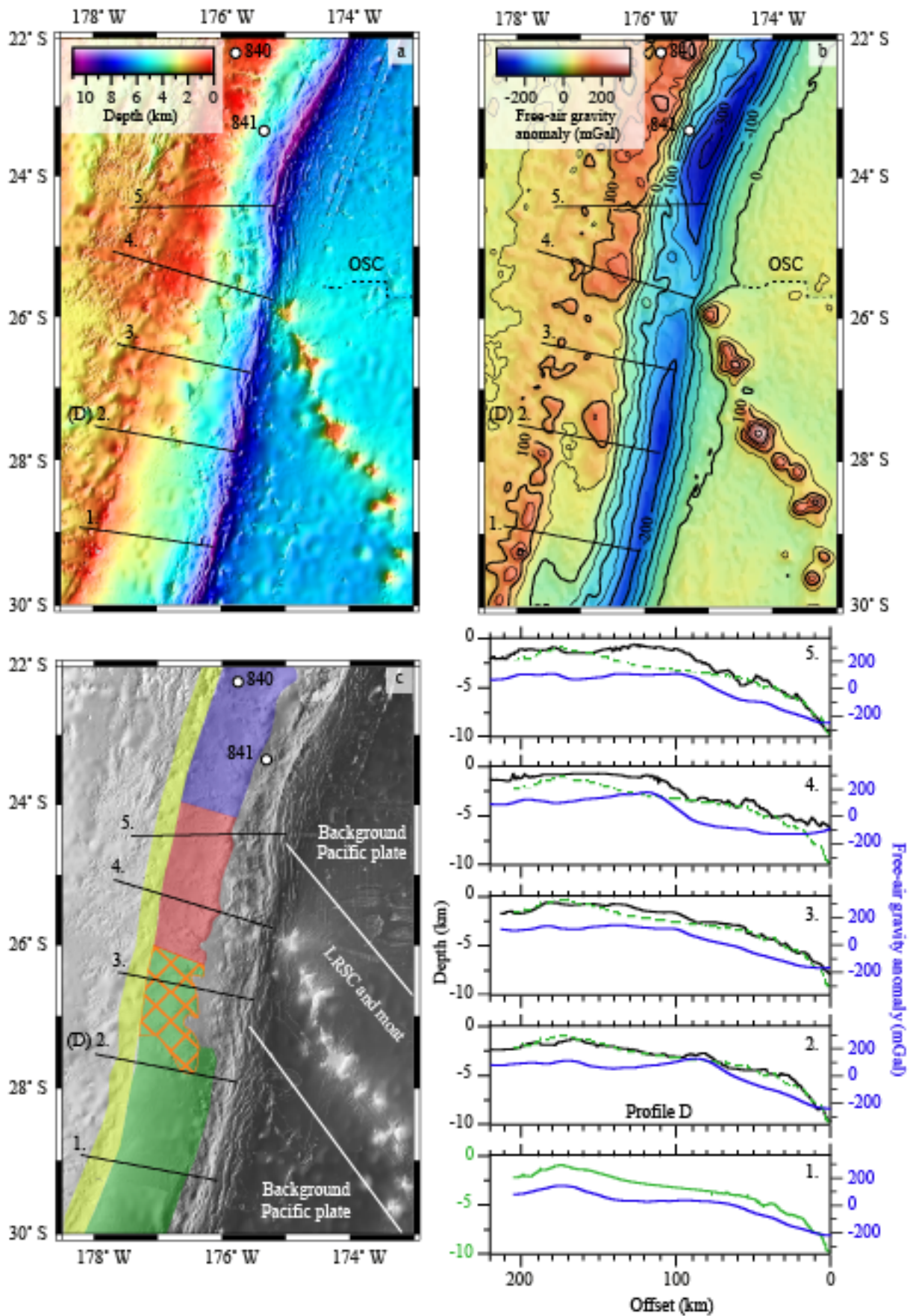
957 **Figure 7**



958

959

960 **Figure 8**



961

962